GEOPHYSICS, VOL. 84, NO. 5 (SEPTEMBER-OCTOBER 2019); P. S459–S478, 51 FIGS.
10.1190/GEO2018-0411.1

Comparison of the inverse scattering series free-surface multiple elimination (ISS FSME) algorithm with the industry-standard surface-related multiple elimination (SRME): Defining the circumstances in which each method is the appropriate toolbox choice

Chao Ma[1], Qiang Fu[1], and Arthur B. Weglein[1]

ABSTRACT

The industry-standard surface-related multiple elimination (SRME) method provides an approximate predictor of the amplitude and phase of free-surface multiples. This approximate predictor then calls upon an energy-minimization adaptive subtraction step to bridge the difference between the SRME prediction and the actual free-surface multiple. For free-surface multiples that are proximal to other events, the criteria behind energy-minimization adaptive subtraction can be invalid. When applied under these circumstances, a proximal primary can often be damaged. To reduce the dependence on the adaptive process, a more accurate free-surface multiple prediction is required. The inverse scattering series (ISS) free-surface multiple elimination (FSME) method predicts free-surface multiples with accurate time and accurate amplitude of free-surface multiples for a multidimensional earth, directly and without any subsurface information. To quantify these differences, a comparison with analytic data was carried out, confirming that when a free-surface multiple interferes with a primary, applying SRME with adaptive subtraction can and will damage the primary, whereas ISS free-surface elimination will precisely remove the free-surface multiple without damaging the interfering primary. On the other hand, if the free-surface multiple is isolated, then SRME with adaptive subtraction can be a cost-effective toolbox choice. SRME and ISS FSME each have an important and distinct role to play in the seismic toolbox, and each method is the indicated choice under different circumstances.

INTRODUCTION

In the beginning of the paper, it is useful to remind ourselves of the definitions of seismic events based on their travel histories (Weglein et al., 2003). For instance, Figure 1 shows different types of seismic events in marine seismic exploration. In marine seismic exploration, reference waves are *first* defined as waves that travel directly from source to receiver and waves that first travel up to the air-water boundary and then to the receiver. These two types of waves did not experience the subsurface. All other events have experienced the subsurface. *Then*, among the waves that did experience the subsurface, ghost events are defined as the seismic events that begin their propagation histories by traveling up from the source to the air-water boundary (source ghosts) or end their histories by traveling down from the air-water boundary to the receiver (receiver ghosts) or both (source and receiver ghosts). After that, events that begin their history going downward from the source and end their history upward at the receiver are divided into primary and multiple events. Primary events are defined as the events that experience only one upward reflection during their propagation history, whereas multiple events are defined as the events that experience multiple reflections during their propagation history. Multiple events are further divided into free-surface multiples and internal multiples depending on the location of downward reflection between two consecutive upward reflections.

Multiples that have at least one downward reflection at the air-water (for offshore exploration) or air-land (for onshore exploration) surface are called free-surface multiples, whereas multiples that have all of their downward reflections below the air-water or air-land surface are called internal multiples (Weglein et al., 1997).

Manuscript received by the Editor 1 June 2018; revised manuscript received 13 March 2019; published ahead of production 21 June 2019; published online 6 September 2019.
[1]University of Houston, M-OSRP, Physics Department, 617 Science and Research Building 1, Houston, Texas 77204, USA. E-mail: chaoma1988@gmail.com (corresponding author); qiang.fu.email@gmail.com; aweglein@uh.edu.

The order of a free-surface multiple is defined as the number of reflections it has experienced *only* at the air-water or air-land surface. In contrast, the order of an internal multiple is defined by the *total* number of downward reflections below the air-water or air-land surface. These definitions of different event types define a sequence of processing steps.

In principle, only primaries are called upon to determine the structure and to identify subsurface properties (Weglein, 2016, 2018b). To obtain a data set consisting of primaries, all other events need to be predicted and removed. Hence, multiples, along with the reference waves, source ghosts, receiver ghosts, and source-and-receiver ghosts, all need to be predicted and removed from the seismic data to obtain the primary-only input to imaging and inversion methods (Weglein, 2018a). There are two types of primaries and multiples: recorded primaries and multiples and unrecorded primaries and multiples. Recorded multiples can be used to provide an approximate image of an unrecorded primary. Unrecorded multiples must be removed to use a recorded multiple to find an approximate image of an unrecorded primary. Currently, in the petroleum industry, smooth velocity models are used to locate structure and perform amplitude analysis. For a smooth velocity model, multiples will always produce imaging artifacts. Therefore, multiples (recorded and unrecorded) need to be removed first from the reflection data before imaging primaries for processing goals that seek to effectively locate and invert reflections. This paper will confine itself to removing recorded free-surface multiples.

Removing and using multiples are seeking the images of primaries: recorded primaries and unrecorded primaries. As pointed out by Weglein (2018b), the relationship between "removing multiples" and "using multiples" is not adversarial but complementary. This paper belongs to the study of the methods in removing multiples.

The methods for removing multiples have advanced and have become more effective. However, the concomitant industry trend toward ever more complex exploration areas and difficult plays has at times outpaced advances in multiple-attenuation capability. For example, currently, the removal of multiples, especially those that are interfering with primaries, for an unknown and complex multidimensional subsurface, remains a key open issue and is a high-priority challenge for offshore and onshore conventional and unconventional plays. We advocate a toolbox approach, in general, and we seek to understand the place and role that each method within the toolbox plays within the spectrum of different capabilities and responses and how to choose the method that's the best match for the user's specific application and objective. We also advocate adding new options to the toolbox to increase the collection of circumstances that can be addressed.

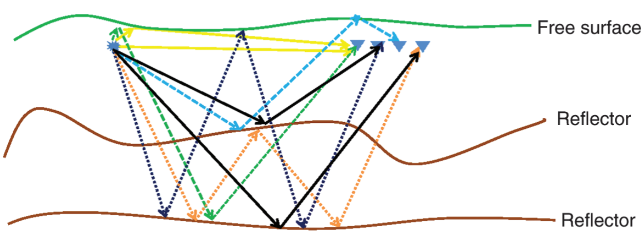

Figure 1. Illustration of different seismic events in the marine environment. Solid yellow line, reference waves; dashed green and light-blue line, source ghost and receiver ghost, respectively; dashed dark-blue line, free-surface multiple; dashed orange line, internal multiple; and solid black line, primary.

In this particular paper, we examine and compare two methods (i.e., inverse scattering series free-surface multiple elimination [ISS FSME] [Carvalho et al., 1991; Weglein et al., 1997, 2003] and surface-related multiple elimination [SRME]) (Berkhout, 1985; Verschuur, 1991; Verschuur et al., 1992) for the removal of *free-surface* multiples. We suggest a guide to when each can be the appropriate choice within the free-surface-multiple-removal toolbox. The SRME method has been widely used and has become (and we expect will remain) the workhorse and industry standard for removing free-surface multiples. Similarly, the effectiveness of ISS FSME has been demonstrated in many complicated synthetic and field data tests (e.g., Carvalho and Weglein, 1994; Matson et al., 1999; Weglein and Dragoset, 2005; Zhang, 2007; Ferreira, 2011).

These free-surface multiple removal methods share a property that both methods do not require subsurface information. However, there are significant and well-documented differences between these two methods as discussed by Weglein et al. (2000) and Weglein and Dragoset (2005). For example, one difference is the SRME method predicts the approximate amplitude and time of free-surface multiples. In contrast, the ISS FSME method predicts free-surface multiples with accurate amplitude and accurate time. There are circumstances in which that difference will be significant and important for removing free-surface multiples without damaging interfering or proximal primaries. The ISS FSME method is more effective and more computationally demanding compared to SRME. There are circumstances in which the added cost is indicated, and other cases in which the lower cost SRME will be the cost-effective choice.

Our aim and single objective is to use examples in 1D with analytic input data to provide a quantitative analysis between two methods in terms of predicting free-surface multiples and removing interfering free-surface multiples without damaging primaries. The outline of the paper is as follows: We first describe ISS free-surface multiple prediction and SRME free-surface multiple prediction. We examine the difference in physics theory that resides behind the different ISS FSME and SRME predictions. After that, we use 1D prestack examples for a quantitative comparison of free-surface multiple prediction between the ISS FSME and SRME methods. We conclude with a discussion and guide for the indicated toolbox choices.

THE ISS FSME ALGORITHM

In this section, we describe the ISS FSME algorithm (Carvalho et al., 1991; Weglein et al., 1997, 2003). We start by first describing the preprocessing steps before ISS FSME and then describing ISS free-surface multiple prediction.

We provide a 2D marine development as an example to illustrate the steps. Given the recorded seismic data (see Figure 1), $D(x_g, x_s, t)$, where x_g, x_s and t represent the receiver and source locations and time, respectively. (1) The first step is to remove the reference waves. (2) After the removal of the reference wave (producing reflection data), the second step is to remove source ghosts, receiver ghosts, and source-and-receiver ghosts that produce deghosted reflection data. (3) After the removal of reference waves and all ghosts (i.e., source ghosts, receiver ghosts, and source-and-receiver ghosts), deghosted seismic reflection data (represented by $D_1'(x_g, x_s, t)$) enter the ISS FSME to predict and remove free-surface multiples as follows:

- $D_1'(x_g, x_s, t)$ is the first Fourier transformed over x_g, x_s, t (i.e., $D_1'(x_g, x_s, t) \rightarrow D_1'(k_g, k_s, \omega)$; see equation A-25 for the Fourier transform convention).
- The Fourier-transformed data, $D_1'(k_g, k_s, \omega)$ enter the ISS free-surface-multiple-prediction equations (i.e., equation 1) to predict free-surface multiples (represented by $D_n'(k_g, k_s, \omega)$, where $n = 2, 3, 4, \ldots$) with accurate time and accurate amplitude (in opposite polarity compared with actual free-surface multiples), of order $n-1$,

$$D_n'(k_g, k_s, \omega) = -\frac{1}{2\pi A(\omega)} \int dk e^{iq(z_g+z_s)} \times D_1'(k_g, k, \omega)(2iq) D_{n-1}'(k, k_s, \omega), \quad n = 2, 3, 4, \ldots. \tag{1}$$

The quantities $A(\omega)$, z_g, and z_s in equation 1 are the source signature, receiver depth, and source depth, respectively, and $q = \sqrt{\omega^2/c_0 - k^2}$.
- Then, these predicted $(n-1)$th order free-surface multiples ($D_n'(k_g, k_s, \omega)$, where $n = 2, 3, 4, \ldots$) are inverse Fourier transformed back to x_g, x_s and t and added to the input data $D_1'(x_g, x_s, t)$ to obtain data without free-surface multiples (see equation 2).

$$D'(x_g, x_s, t) = D_1'(x_g, x_s, t) + D_2'(x_g, x_s, t) + D_3'(x_g, x_s, t) + \cdots, = \sum_{n=1}^{\infty} D_n'(x_g, x_s, t). \tag{2}$$

It should be mentioned that the subsequent prediction terms in the series (equation 2), represented by D_2', D_3', ..., provide predictions of free-surface multiples of different orders. Specifically, each term in D_n' (where $n = 2, 3, 4, \ldots$) when added to the earlier terms in the series (including the data D_1') performs two functions: (1) It eliminates the nth-order free-surface multiple, and (2) it alters all higher-order free-surface multiples to be prepared for their removal by higher order D_j' terms, where $j = n+1, n+2, \ldots$ (Weglein et al., 2003; Zhang and Shaw, 2010; Ma and Weglein, 2016). The output of the ISS FSME $D'(x_g, x_s, t)$ represents the data without reference waves, without all ghosts, and without free-surface multiples.

SRME

The 2D SRME free-surface multiple prediction, denoted by M (Berkhout, 1985; Verschuur, 1991; Verschuur et al., 1992), is calculated by using seismic data without reference waves and receiver-side ghosts, but retaining source-side ghosts, denoted by P, as follows:

$$M(x_g, x_s, \omega) = \int P(x_g, x, \omega) P(x, x_s, \omega) dx, \tag{3}$$

where x_g, x_s, ω are the receiver and source locations and temporal frequency, respectively. To obtain equation 3, one would have to assume in the physics derivation that the data were generated by a vertically separated dipole source in the water column (with the reference wave and source and receiver ghosts removed [see the details in Appendix B]). The actual monopole source itself together with its source ghost (corresponding to a mirror image [in the air above the sea surface] of the actual monopole source in the water) is assumed in the SRME prediction step to be an approximation to the dipole source in the water column.

The physics theory differences between these two free-surface multiple-prediction algorithms are studied in Appendices A and B. In the next section, we focus on a quantitative comparison between the ISS and SRME free-surface multiple predictions.

A QUANTITATIVE COMPARISON BETWEEN THE ISS AND SRME FREE-SURFACE MULTIPLE PREDICTIONS

In this section, we aim to provide a quantitative comparison between ISS free-surface multiple prediction and SRME free-surface multiple prediction.

From the last section, we know that the called-for input data to the two free-surface multiple-prediction algorithms are different. The input seismic data for the ISS FSME algorithm are generated by a monopole source with the reference wave and all ghosts removed (see Figure 2). For SRME, the input is seismic data generated by a dipole source with the reference wave and ghosts removed. However, in practice, because the data due to a vertically separated dipole source are not realizable, the assumption made within SRME is to approximate what a dipole source in the water would produce by a monopole source and its source-side ghost (in the air).

Following that, in the first set of comparisons (see the first bullet in Figure 3), we provide different called-for inputs to these

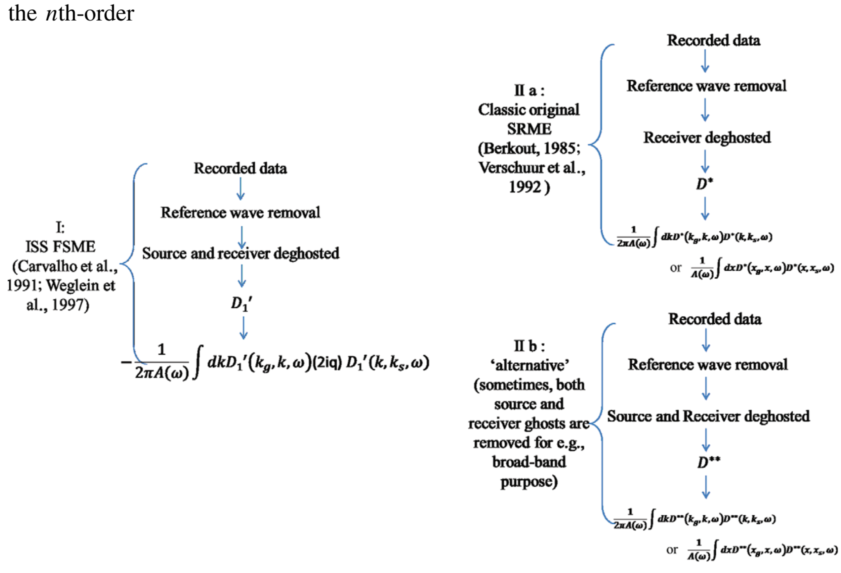

Figure 2. The ISS free-surface multiple prediction algorithm and the SRME free-surface multiple prediction algorithm.

two free-surface multiple-prediction algorithms. For the ISS free-surface multiple-prediction algorithm, we use data due to a monopole source with the reference wave and all ghosts removed. Similarly, for the SRME free-surface multiple-prediction algorithm, we use data due to a monopole source with the reference wave and the receiver-side ghosts removed (source-side ghosts are retained in the data).

Ghosts can have a detrimental effect on seismic bandwidth and resolution. Therefore, in practice, source and receiver ghosts are often removed early in the processing chain prior to multiple removal processing taking place. Hence, we carry out the second set of comparisons with input data with the reference wave and all ghosts removed for both algorithms. The latter tests are carried out with and without noise (see the second and third bullets in Figure 3).

In the third set of comparisons, we repeat the previous comparison, with input data generated by an absorptive medium (see the fourth bullet in Figure 3). We aim to examine whether, for input data generated by an absorptive medium, the two free-surface multiple-prediction algorithms retain their relative and different levels of effectiveness; i.e., the ISS predicts free-surface multiples with accurate amplitude and time, and the SRME predicts free-surface multiples with approximate amplitude and approximate time in the presence of an absorptive medium.

Weglein et al. (2003, pp. R52–R55) provide proof that the ISS FSME method predicts the precise time and amplitude of all free-surface multiples, without any subsurface information and is independent of the earth model type. Similarly, Weglein et al. (2003, pp. R55–R62) also show that the ISS internal multiple attenuator predicts the precise time and approximate amplitude of all internal multiples, without subsurface information and is independent of the earth model type.

The first set of comparisons

In this first set of comparisons, given the required input of these two free-surface multiples algorithms, we provide a quantitative comparison of the predicted free-surface multiples by the ISS FS and the SRME methods. In other words, for ISS free-surface multiple prediction, the input data are without reference waves and without all ghosts; for SRME free-surface multiple prediction, the input data are without the reference wave and receiver ghosts (the source ghosts are retained in its input data).

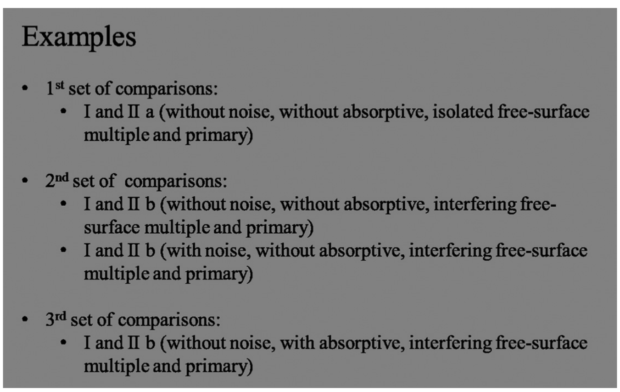

Figure 3. Three sets of comparisons between the ISS free-surface multiple prediction and the SRME free-surface multiple prediction.

Figure 4 shows the model with one horizontal reflector and a free surface. Based on this model, we use the Cagniard-de Hoop (CdH) method (Cagniard, 1939; de Hoop, 1959) to generate the data. For a model with one horizontal reflector and a free surface, the CdH method is able to obtain the analytical solutions of different events separately. This allows us to generate data according to each algorithm's required input and to attribute any difference in the comparison to the two prediction algorithms rather than to numerical or other issues with the data. Figures 5 and 6 show the inputs to the ISS and SRME free-surface multiple predictions, respectively. Figures 7 and 8 show the prediction results from ISS and SRME. For the ISS free-surface multiple prediction, we use equation 1 for $n = 2$ (for first-order free-surface multiples). Figures 9 and 10 show the trace comparison at a 500 m offset between the input data and the free-surface multiple predictions from ISS and SRME, respectively. The results show that ISS FSME predicts free-surface multiples with accurate time and amplitude, whereas SRME predicts free-surface multiples with approximate time and amplitude.

The second set of comparisons

Figure 11 shows the model we used to generate analytic input data in the (k_x, ω) domain for a 1D subsurface (using the reflectivity

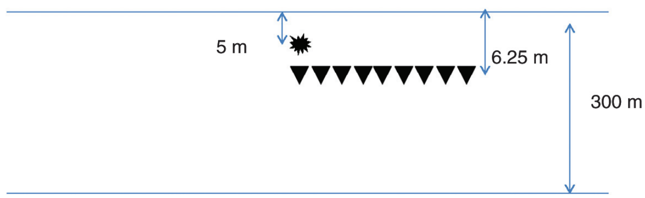

Figure 4. A 1D subsurface model with a horizontal reflector and a free surface.

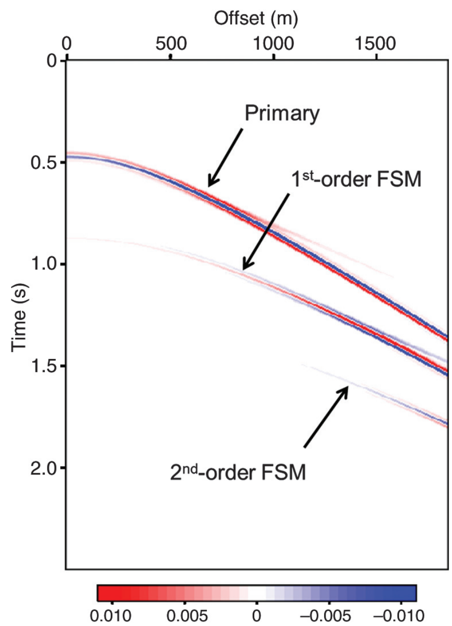

Figure 5. Input data for the ISS free-surface multiple prediction. Note that only primaries and free-surface multiples are generated for ISS FSME input.

method). For example, a primary due to a horizontal reflector has the analytic form shown below (see, e.g., Stolt and Weglein, 1985):

$$-R(k_x,\omega)\frac{e^{iq(2a-z_g-z_s)}}{2iq}, \tag{4}$$

where $R(k_x,\omega)$, a, z_g and z_s are the plane-wave reflection coefficient, depths of the reflector, receiver, and source, respectively; $q=\sqrt{\omega^2/c_0^2-k_x^2}$, where c_0 is the velocity above the reflector. For this model, the above expression for a primary can be generalized to generate other events analytically. A Ricker wavelet with a peak frequency at 30 Hz is convolved with the analytic form to generate the data.

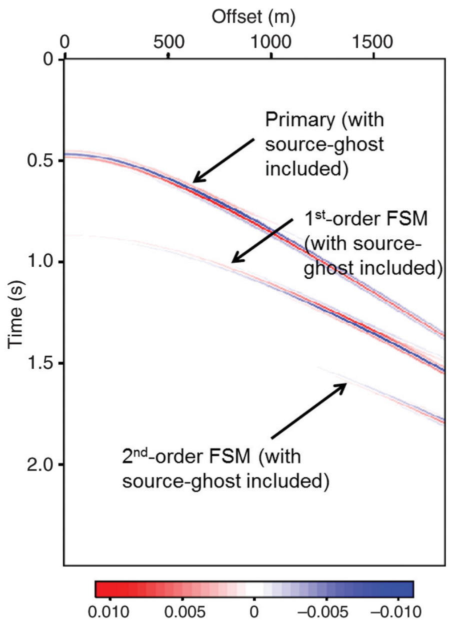

Figure 6. Input data for the SRME free-surface multiple prediction. Note that primaries and free-surface multiples and their source ghosts are generated for SRME input.

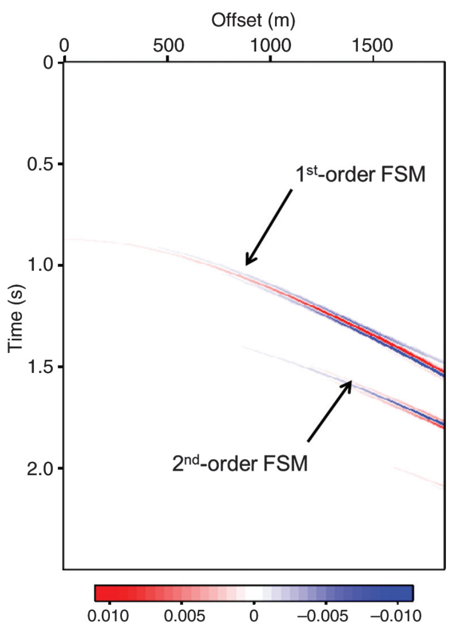

Figure 7. ISS free-surface multiple prediction (D_2' in equation 1) with the input in Figure 5.

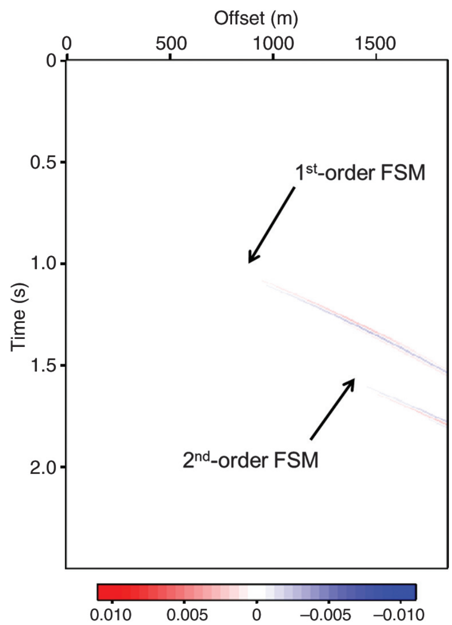

Figure 8. SRME free-surface multiple prediction (equation 3) with the input in Figure 6.

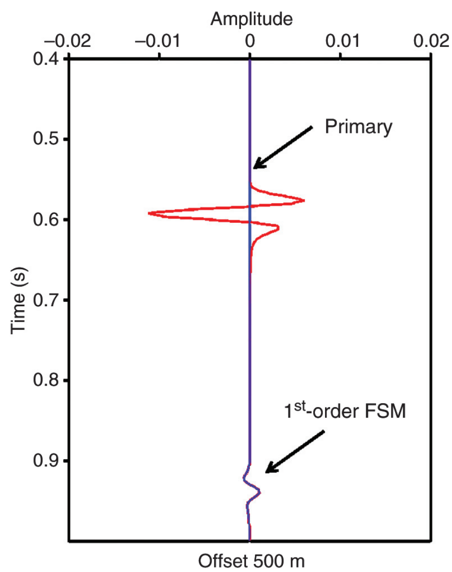

Figure 9. A trace comparison at a 500 m offset between the input of the ISS FSME and its prediction. The red and blue lines represent input data to the ISS FSME and its prediction, respectively. We can see that the ISS free-surface multiple prediction agrees with the actual free-surface multiple very well. Note that the predicted free-surface multiple has an opposite sign compared with the actual free-surface multiple, we first flip the polarity of the prediction and then compare it with the actual data for easy comparison.

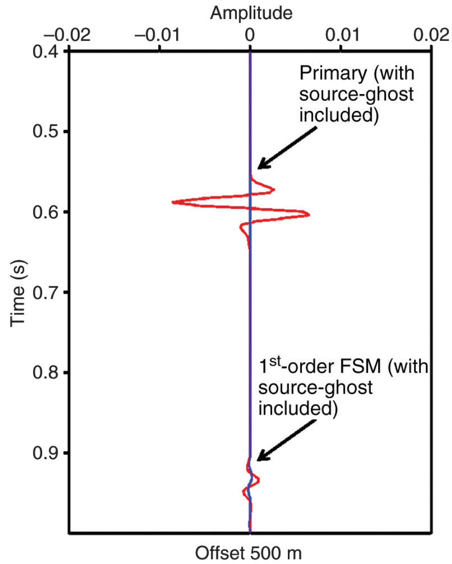

Figure 10. A trace comparison at a 500 m offset between the input of the SRME and its prediction. The red and blue lines represent the input data to the SRME and its prediction for free-surface multiples, respectively. We can see from this trace comparison that the SRME provides an approximate free-surface multiple prediction.

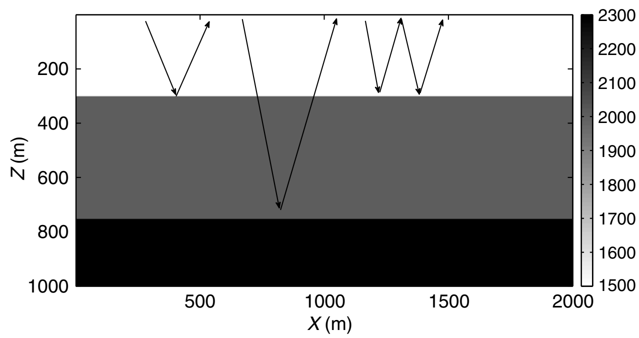

Figure 11. A 1D subsurface model with two primary events and one free-surface multiple event.

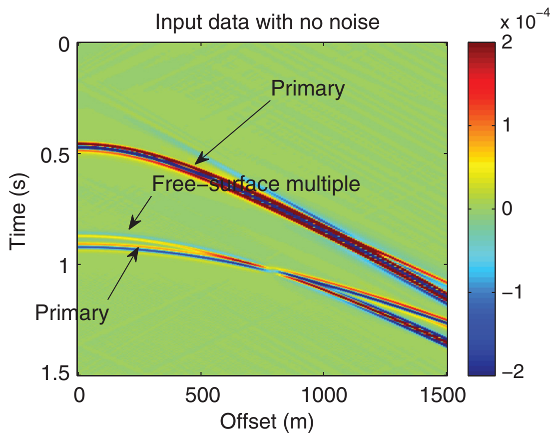

Figure 12. Input data generated based on the model shown in Figure 11.

In our example, (1) only three events (two primaries and one free-surface multiple) are generated and (2) the depths of the reflectors and velocities are chosen such that the second primary destructively interferes with the free-surface multiple. We examine two cases using input data with and without random noise. The only difference between these two tests is the input data; the input data for test 1 contains no noise, whereas the input data for test 2 contains random noise.

Figures 12, 13, 14, 15, and 16 show the synthetic input data, ISS free-surface multiple prediction, SRME free-surface multiple prediction, results after the ISS FSME and SRME + adaptive, and the actual primary, respectively. For the predictions of free-surface multiples in Figures 13 and 14, higher order free-surface multiples (as we know) are also predicted and that the result from ISS FSME was obtained by directly subtracting the ISS prediction result from the data without an adaptive procedure, whereas the result from SRME was obtained by combining the SRME free-surface multiple prediction and the adaptive procedure.

Comparing the primary in the data (Figure 17) with the multiple-removal result after ISS FSME (Figure 15), we find that, with accurate multiple prediction, the ISS FSME has precisely removed the free-surface multiple and recovered the primary.

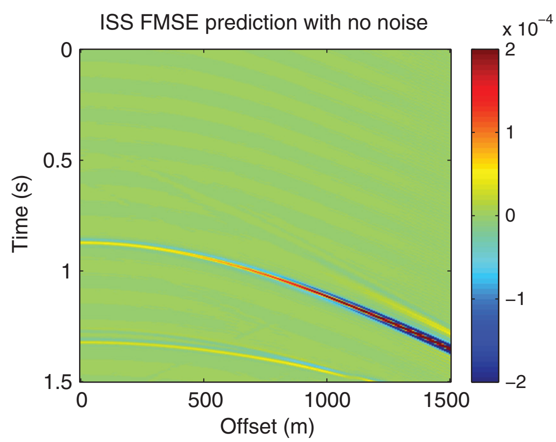

Figure 13. Prediction of a free-surface multiple by ISS FSME (D_2' in equation 1) using the input data shown in Figure 12.

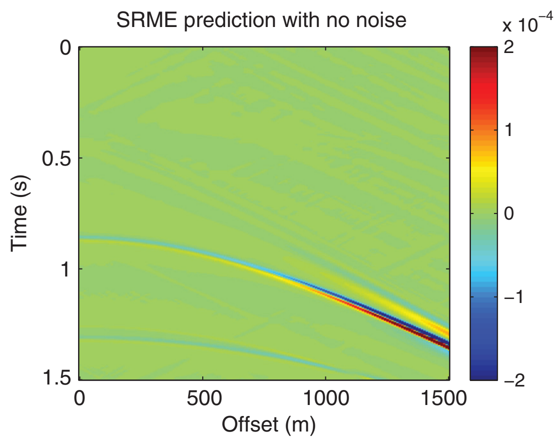

Figure 14. Prediction of a free-surface multiple by SRME using the input data shown in Figure 12.

Comparing the original data (Figure 12) with the result after SRME + adaptive (Figure 16), we noted that SRME can successfully remove the isolated multiple. The isolated free-surface multiple in Figure 12 is removed in Figure 16. In Figure 16, the arrows point to the removed free-surface multiple. However, the adaptive procedure can easily damage the primary, which interferes with the multiple (the red circle in Figure 16). It is worth mentioning that we used least-squares (L2-norm) energy minimization adaptive subtraction, which is a current standard practice in the industry, to remove the predicted free-surface multiple event from the data in Figure 16.

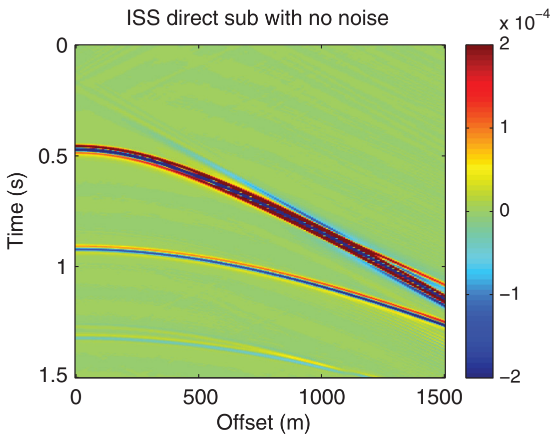

Figure 15. Free-surface multiple removal result after directly subtracting the ISS prediction result (Figure 13) from the data (Figure 12).

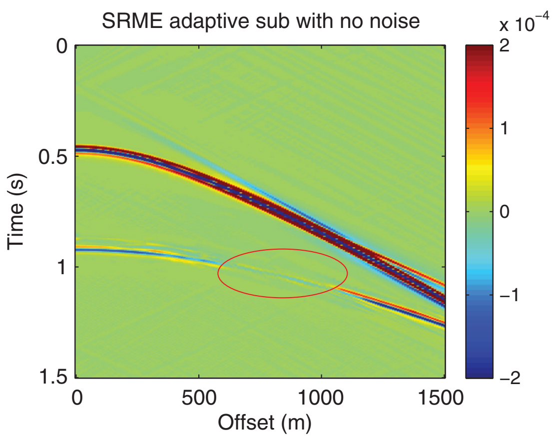

Figure 16. Free-surface multiple removal result by combining the SRME prediction (Figure 14) and adaptive subtraction.

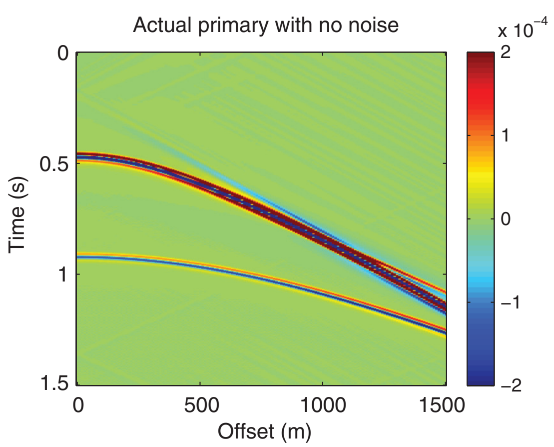

Figure 17. Actual primaries in the data shown in Figure 12.

Figures 18, 19, 20, 21, and 22 provide trace plots to examine the results in detail at different offsets. In these trace plots, the red, blue, and green lines represent the actual data, ISS FSME multiple prediction, and SRME multiple prediction, respectively. In the 100, 500, 1000, and 1250 m offset trace plots, primaries and multiples are separated from each other. These plots show that ISS free-surface multiple prediction has an accurate time and amplitude, hence, it overlaps with the actual multiples in the data, whereas SRME prediction has approximate amplitude and time and it shows disagreement with the actual multiple in the data.

At offset 750 m, the primary and multiple overlap. Figure 23 shows a comparison between the actual primary (blue line) with the

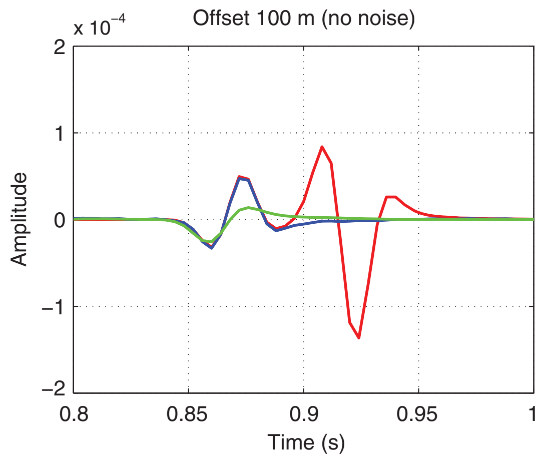

Figure 18. Trace comparison at offset 100 m. The red, blue, and green lines represent actual data, ISS free-surface multiple prediction, and SRME prediction, respectively.

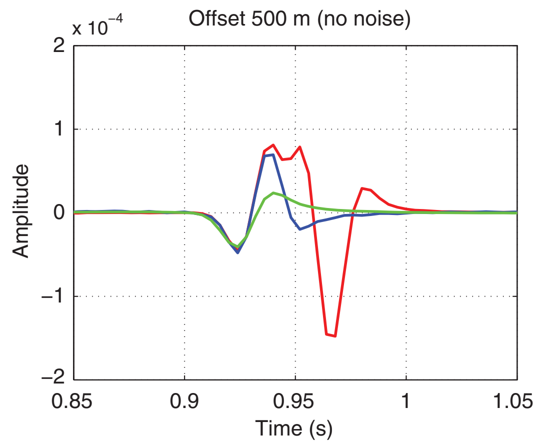

Figure 19. Trace comparison at offset 500 m. The red, blue, and green lines represent actual data, ISS free-surface multiple prediction, and SRME prediction, respectively.

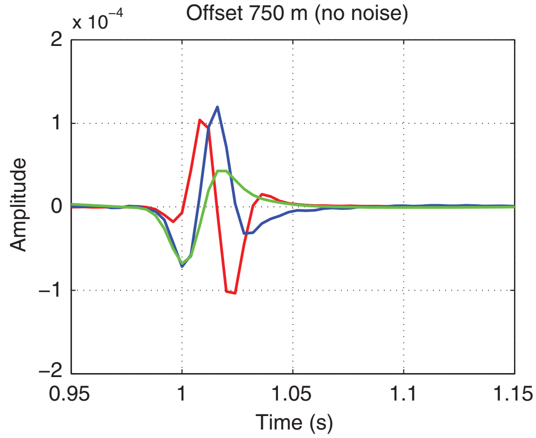

Figure 20. Trace comparison at offset 750 m. The red, blue, and green lines represent actual data, ISS free-surface multiple prediction, and SRME prediction, respectively.

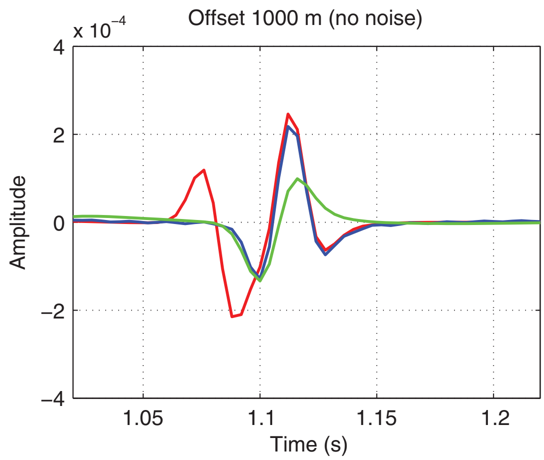

Figure 21. Trace comparison at offset 1000 m. The red, blue, and green lines represent actual data, ISS free-surface multiple prediction, and SRME prediction, respectively.

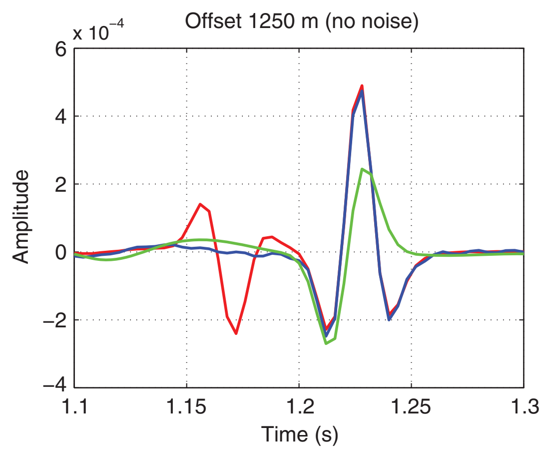

Figure 22. Trace comparison at offset 1250 m. The red, blue, and green lines represent actual data, ISS free-surface multiple prediction, and SRME prediction, respectively.

multiple-removal result after ISS FSME (the red line) and the multiple-removal result after SRME + adaptive (the green line) at offset 750 m. This figure shows that the primary can be recovered by ISS FSME, whereas the SRME combined with the adaptive damages the primary.

For test 2, in which the input data have random noise, Figures 24, 25, 26, 27, 28, and 29 show the synthetic input data, multiple prediction results from ISS FSME, SRME, results after the ISS FSME and SRME + adaptive, and the actual primary, respectively. Similarly, Figures 30, 31, 32, 33, 34, and 35 provide trace plots. Examining these comparisons, we can draw a similar conclusion as in the case without noise.

The third set of comparisons

Weglein et al. (2003) show the model-type independent properties of the ISS FSME algorithm and the internal multiple attenuation algorithm. The meaning of model-type independent is that the removal of free-surface multiples and the attenuation of internal multiples is each achievable with precisely the same algorithm for an entire class of earth model types. The members of the models' type class include acoustic, elastic, and anelastic media. Matson (1997)

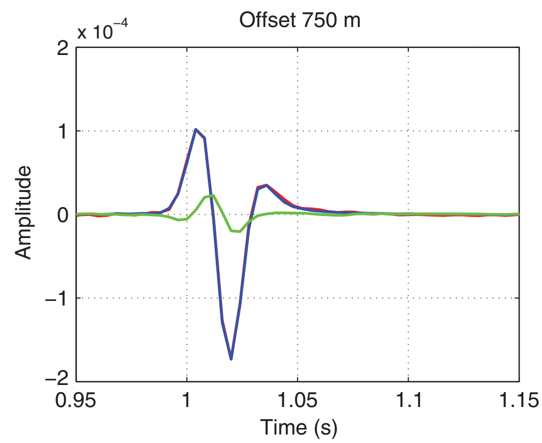

Figure 23. Trace comparison at offset 750 m. The red, blue, and green lines represent the actual primary, result after ISS FSME, and result after the SRME + adaptive, respectively.

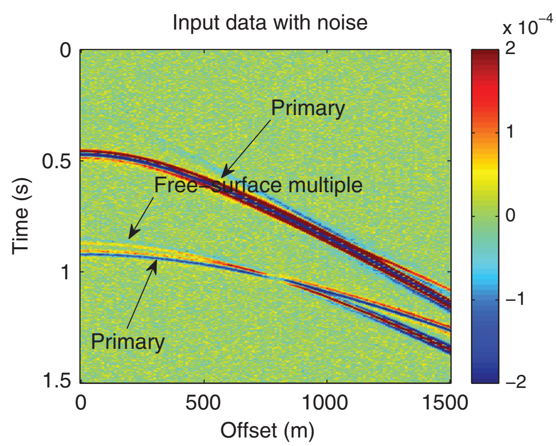

Figure 24. Input data with random noise added to the analytic data.

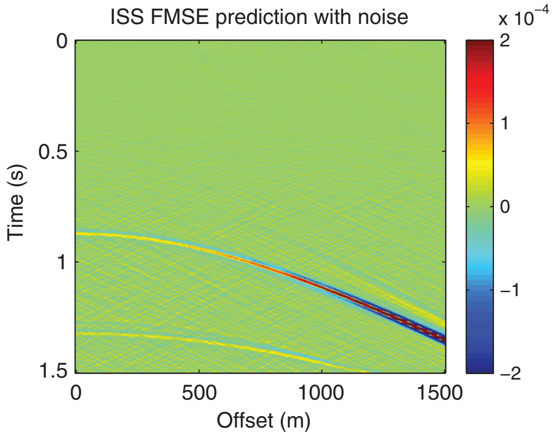

Figure 25. Prediction of a free-surface multiple by ISS FSME (D_2' in equation 1) using the input data shown in Figure 24.

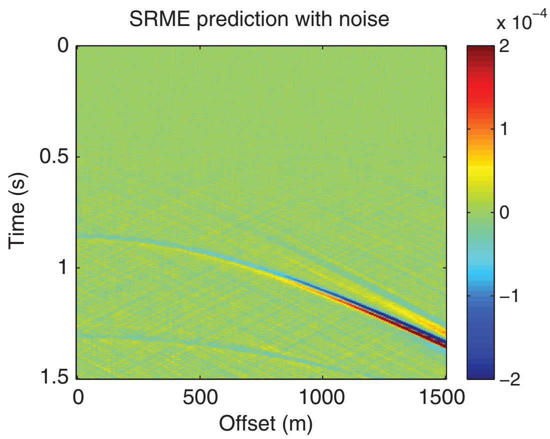

Figure 26. Prediction of a free-surface multiple by SRME using the input data shown in Figure 24.

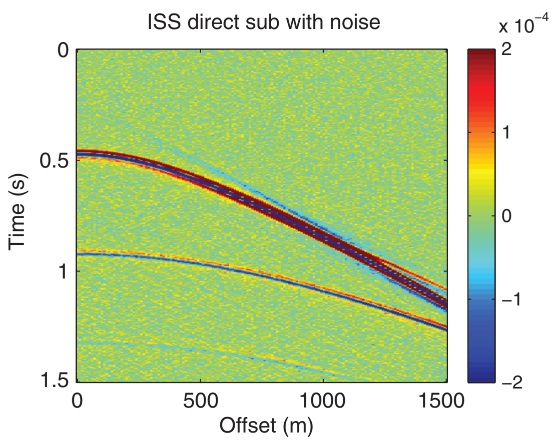

Figure 27. Free-surface multiple removal result after directly subtracting the ISS prediction result (Figure 25) from the data (Figure 24).

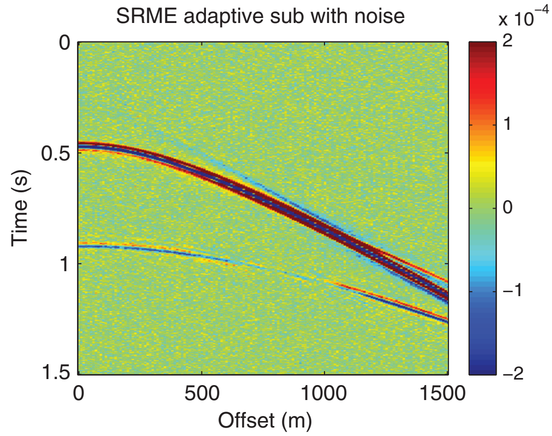

Figure 28. Free-surface multiple removal result by combining the SRME prediction (Figure 26) and adaptive subtraction.

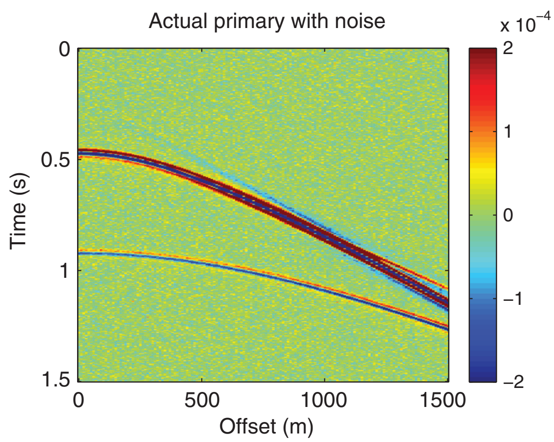

Figure 29. Actual primaries in the data shown in Figure 24.

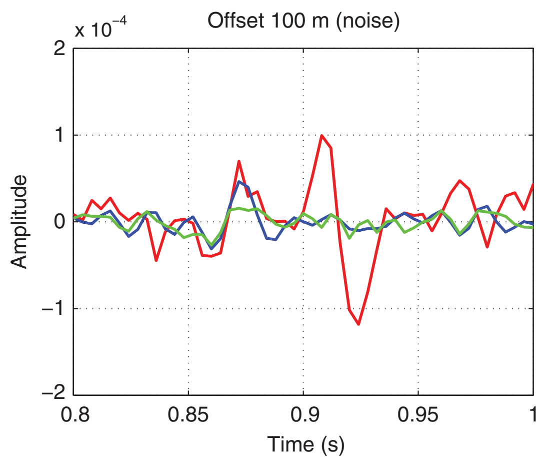

Figure 30. Trace comparison at an offset of 100 m. The red, blue, and green lines represent the actual data, ISS free-surface multiple prediction, and SRME prediction, respectively.

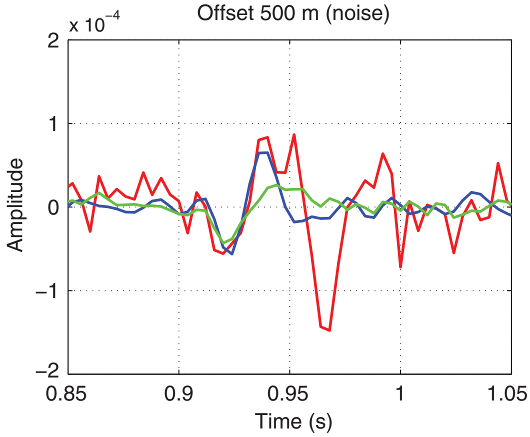

Figure 31. Trace comparison at an offset of 500 m. The red, blue, and green lines represent the actual data, ISS free-surface multiple prediction, and SRME prediction, respectively.

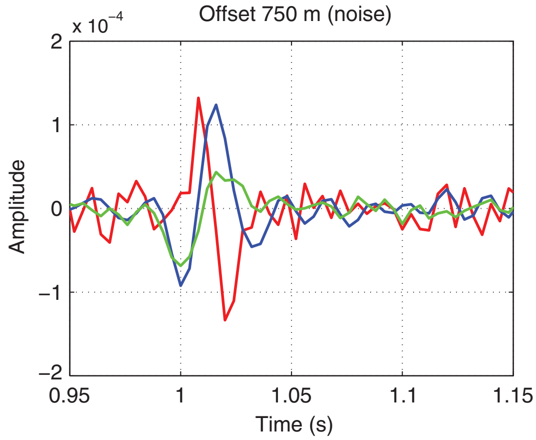

Figure 32. Trace comparison at an offset of 750 m. The red, blue, and green lines represent the actual data, ISS free-surface multiple prediction, and SRME prediction, respectively.

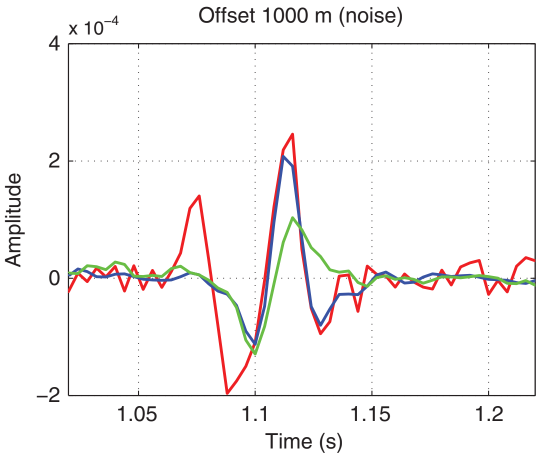

Figure 33. Trace comparison at an offset of 1000 m. The red, blue, and green lines represent the actual data, ISS free-surface multiple prediction, and SRME prediction, respectively.

studies and demonstrates the effectiveness of ISS elastic multiple removal from multicomponent land and ocean-bottom seismic data. Here, we provide a numerical example to demonstrate and confirm the effectiveness of the ISS FSME algorithm for an absorptive medium.

The input data are generated based on the model shown in Figure 11, with Q values 200, 100, and 100 for the three layers from top to bottom. The analytic input data are generated using the analytic forms of different events (see, e.g., equation 4 for a primary) and a constant Q model (known as the frequency-independent Q model) (see Kolsky, 1956). Figures 36, 37, and 38 show the input data, ISS free-surface multiple prediction, and SRME free-surface multiple prediction, respectively. Figures 39, 40, and 41 show the result after the ISS FSME, SRME + adaptive and actual primary in the data, respectively. Figures 42, 43, 44, 45, and 46 show the trace comparison among the input data, ISS free-surface multiple prediction, and SRME free-surface multiple prediction at offsets of 100, 500, 750, 1000, and 1250 m. Figure 47 shows the trace comparison at offset 750 m between the actual primary, the result after the ISS

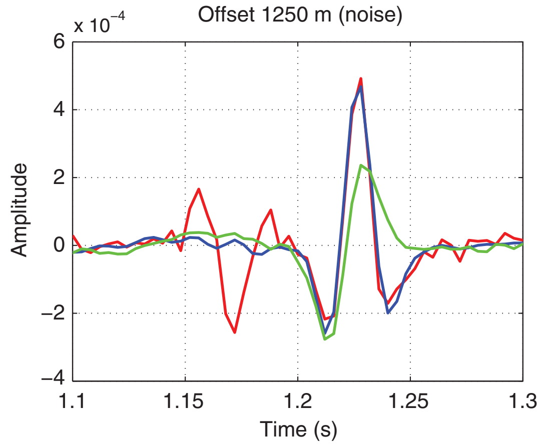

Figure 34. Trace comparison at an offset of 1250 m. The red, blue, and green lines represent the actual data, ISS free-surface multiple prediction, and SRME prediction, respectively.

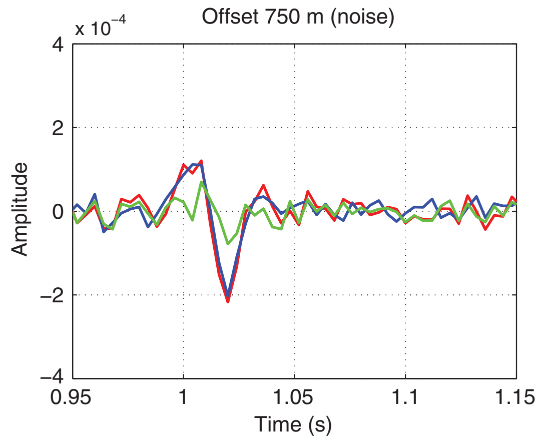

Figure 35. Trace comparison at an offset of 750 m. The red, blue, and green lines represent the the actual primary, result after ISS FSME, and result after the SRME + adaptive, respectively.

FSME, and the result after the SRME + adaptive. Examining the result of this test, we can conclude that, for data generated by an acoustic medium that's absorptive, the same ISS FSME algorithm remains effective to accurately predict the free-surface multiple and can surgically remove free-surface multiples that interfere with primaries, without damaging the primaries. We have numerically confirmed that the ISS FSME algorithm remains effective with data

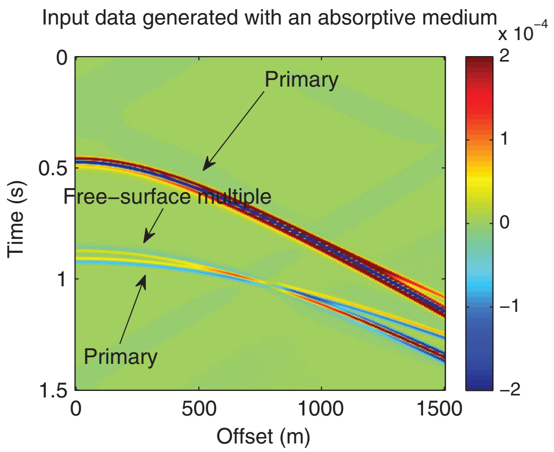

Figure 36. Input data generated from an absorptive medium.

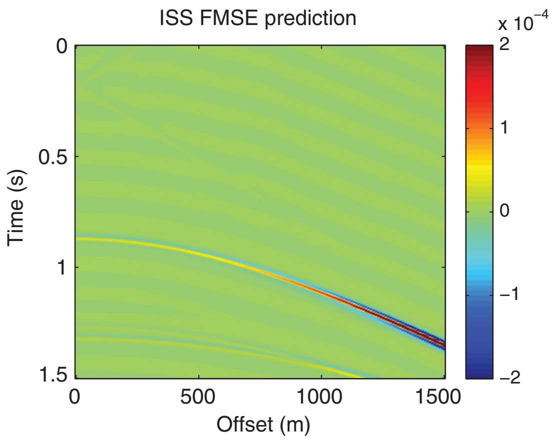

Figure 37. Prediction of a free-surface multiple by ISS FSME (D_2' in equation 1) using the input data generated by an absorptive medium shown in Figure 36.

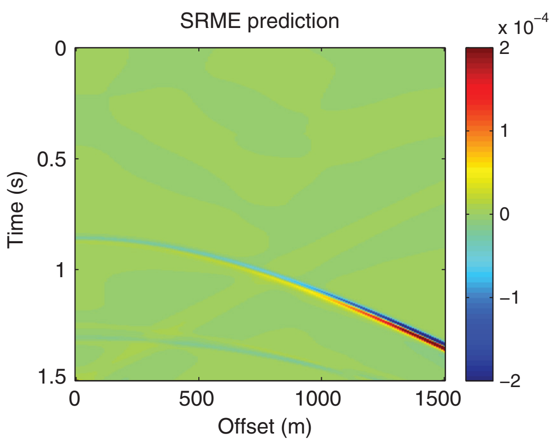

Figure 38. Prediction of a free-surface multiple by SRME using the input data generated by an absorptive medium shown in Figure 36.

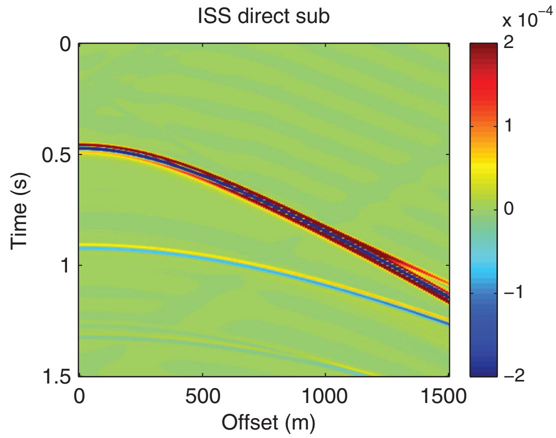

Figure 39. Free-surface multiple removal result after directly subtracting the ISS prediction result (Figure 37) from the data (Figure 36).

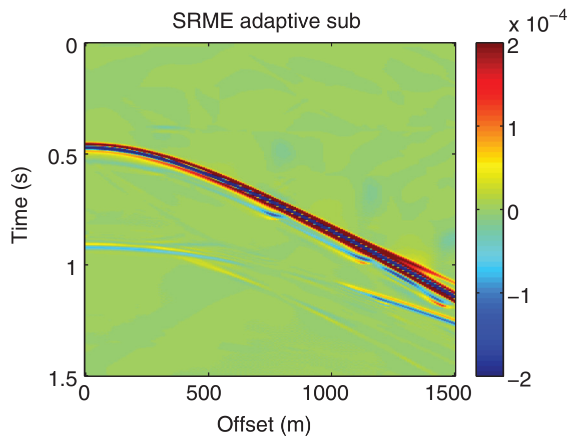

Figure 40. Free-surface multiple removal result by combining the SRME prediction (Figure 38) and adaptive subtraction.

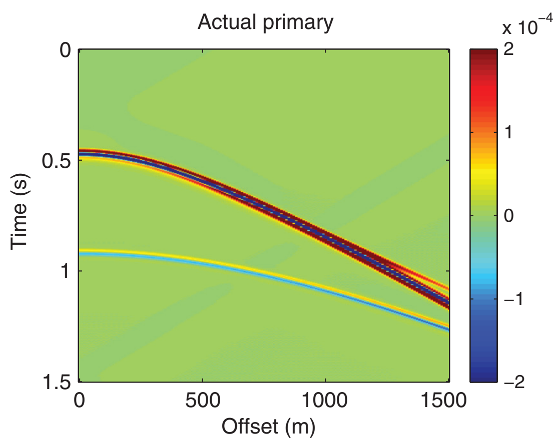

Figure 41. Actual primaries in the input data shown in Figure 36.

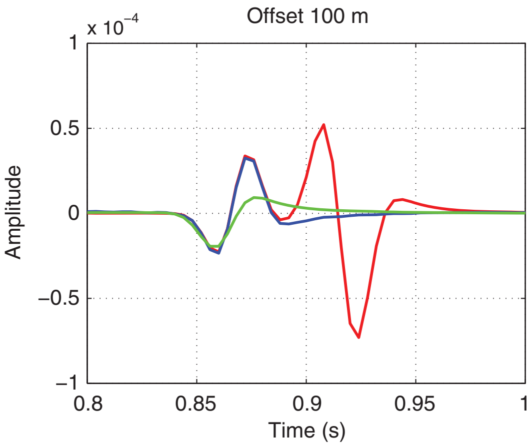

Figure 42. Trace comparison at offset 100 m. The red, blue, and green lines represent the actual data, ISS free-surface multiple prediction, and SRME prediction, respectively.

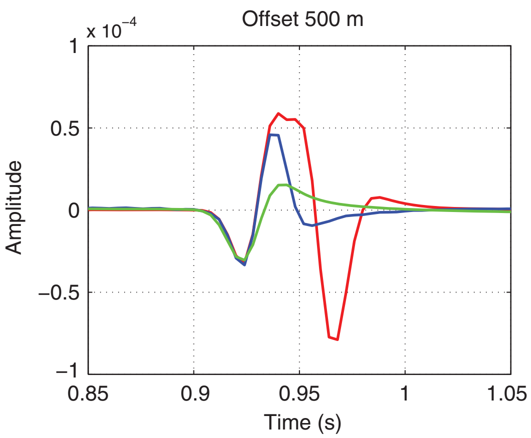

Figure 43. Trace comparison at offset 500 m. The red, blue, and green lines represent the actual data, ISS free-surface multiple prediction, and SRME prediction, respectively.

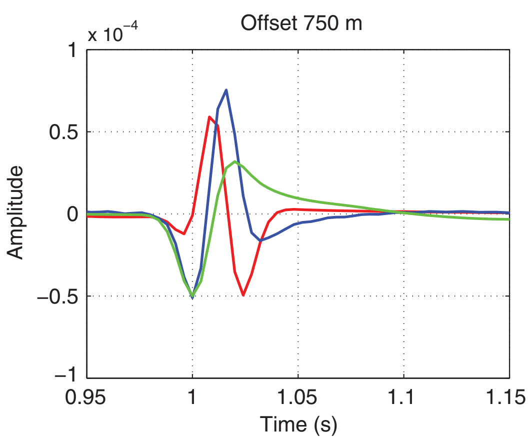

Figure 44. Trace comparison at offset 750 m. The red, blue, and green lines represent the actual data, ISS free-surface multiple prediction, and SRME prediction, respectively.

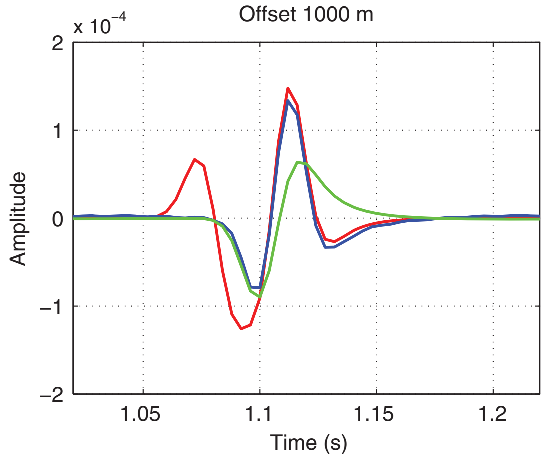

Figure 45. Trace comparison at offset 1000 m. The red, blue, and green lines represent the actual data, ISS free-surface multiple prediction, and SRME prediction, respectively.

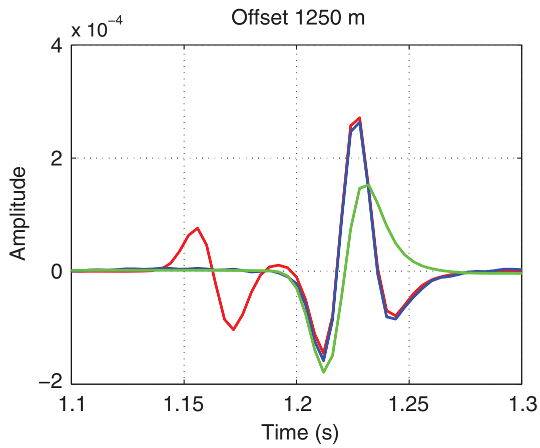

Figure 46. Trace comparison at offset 1250 m. The red, blue, and green lines represent the actual data, ISS free-surface multiple prediction, and SRME prediction, respectively.

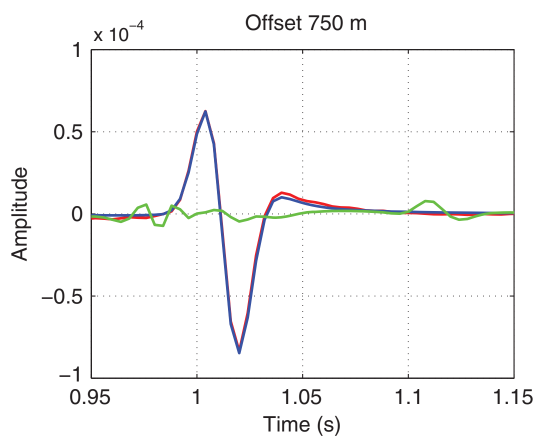

Figure 47. Trace comparison at offset 750 m. The red, blue, and green lines represent the actual primary, result after ISS FSME, and result after the SRME + adaptive, respectively.

from an absorptive medium. That result is consistent with the model type independent nature of the algorithm.

ISS FSME is more computational costly than SRME. The ISS free-surface multiple prediction equation is in the wavenumber-frequency domain; the obliquity factor in it $(2iq)$ precludes a simple transform from the wavenumber-frequency to the space-frequency domain to obtain a convolutional equation (which is cheaper) as in SRME free-surface multiple prediction.

DISCUSSION

Providing prerequisites of the ISS FSME algorithm

ISS FSME has well-understood prerequisites: source signature estimation and removal, removal of the reference wave, and source and receiver-side deghosting. Providing these prerequisites is relatively mature for marine applications. Advances in acquisition (e.g., over/under the cable and the dual-sensor towed streamer) have provided the data requirements of more effective wave theoretic methods for those prerequisites. For example, Weglein and Secrest (1990), Osen et al. (1998), and Tan (1999) provide effective methods to estimate the source signature and radiation pattern using Green's theorem. For prediction (and use or removal) of the reference waves, there are distinct advantages (e.g., [1] there is no need for Fourier transforms over the receivers and sources and [2] it can accommodate a horizontal or nonhorizontal measurement surface). Applying Green's theorem wave separation methods on marine data has been advanced by Weglein et al. (2002), Zhang (2007), and Mayhan and Weglein (2013). For deghosting, the industry's widely used $P-V_z$ method (e.g., Amundsen, 1993) can be effective when the measurement surface is horizontal. The Green's theorem-based deghosting method (Weglein et al., 2002; Zhang, 2007; Mayhan, 2013) is the natural Green's theorem wave theoretic generalization of $P-V_z$, and it has been extended to accommodate a depth-variable cable by the recent work of Wu and Weglein (2017), Zhang (2017), and Shen (2017). To provide the prerequisites for onshore application, the recent work of Wu and Weglein (2014, 2015, 2016a, 2016b) has contributed to extending off-shore Green's theorem preprocessing for wavelet estimation, reference waves (including ground roll) prediction and removal, and deghosting to the on-shore elastic case, in preparation for on-shore processing.

New adaptive criteria that aligned with the algorithm itself

We have shown that, given its prerequisites, ISS FSME will predict free-surface multiples with an accurate time and an accurate amplitude. These predicted multiples can be used to surgically remove free-surface multiples that interfere with primaries, without damaging the primaries. In practice, an adaptive step could still be needed. The energy minimization criteria are viewed (by some thoughtful individuals) as the biggest current impediment to effective multiple removal under complex circumstances. New adaptive criteria need to be developed. We are developing new adaptive criteria derived as a property of the multiple removal algorithm. Candidate criteria are proposed by Weglein (2012).

CONCLUSION

We examined the origin of the missing obliquity factor in the SRME prediction step. We then used 1D prestack examples for a quantitative comparison of free-surface multiple prediction between the ISS FSME and SRME methods. The ISS FSME method provides a toolbox capability and an option for a more accurate prediction of free-surface multiples. There are circumstances in which this new and more effective capability might not be needed. For example, to remove isolated free-surface multiples, an approximate free-surface multiple prediction plus an adaptive subtraction by the SRME method might be sufficient and may be indicated as a cost-effective approach. However, there are many circumstances in which this new ISS FSME capability is called-for and needed. For example, (1) to remove a free-surface multiple that is interfering with a primary without damaging the primary, by providing a more accurate free-surface multiple prediction and relying less on the adaptive step. (2) And when it is unclear if a free-surface multiple is (or is not) interfering with a primary, ISS FSME would be a prudent choice. When this capability is needed, the ISS FSME method provides an important and valuable option in the toolbox. It goes without saying that for the SRME and ISS FSME methods to deliver on their promises, they must be applied in their 2D and 3D versions, in which the subsurface has 2D and 3D variability.

ISS methods for attenuating or eliminating internal multiples place a high bar on not having residual free-surface multiples or damaged primaries in the data. If ISS internal multiple removal is the goal, we suggest a serious consideration of the most effective method for removing free-surface multiples, ISS FSME.

ACKNOWLEDGMENTS

We would like to thank the M-OSRP sponsors for their support and encouragement. The reviewers of this paper are thanked for their constructive and worthwhile comments and suggestions. We thank J. Mayhan for his help in editing this paper.

DATA AND MATERIALS AVAILABILITY

Data associated with this research are available and can be obtained by contacting the corresponding author.

APPENDIX A

THE ISS AND ITS SUBSERIES FOR FSME

In this section, we provide a derivation of the ISS FSME method. Toward that end, we begin with (following Weglein et al., 2003) a very brief introduction and background on scattering theory and the distinct forward and ISS. A fuller development of the concepts and methods in this appendix can be found in Weglein et al. (2003) and Weglein (2018).

The seismic forward problem

The seismic forward-modeling problem is to predict the wavefield in a medium when the medium properties that govern wave propagation in the medium and the source that generates the wavefield are prescribed. For example, for an acoustic, one-parameter (variable velocity, constant density) medium, the single-frequency wave equation for the pressure field due to a localized Dirac delta function source at $\mathbf{r}_s$ is

$$[\nabla^2 + k^2]G(\mathbf{r},\mathbf{r}_s,\omega) = -\delta(\mathbf{r}-\mathbf{r}_s), \tag{A-1}$$

where $k = \omega/c(\mathbf{r})$, ω is the temporal frequency, and $c(\mathbf{r})$ is the velocity configuration. The wavefield $G(\mathbf{r}, \mathbf{r}_s, \omega)$ at $\mathbf{r}$ due to source at $\mathbf{r}_s$ can be modeled directly in terms of the actual velocity configuration $c(\mathbf{r})$ using, e.g., a finite difference, finite element, and lattice Boltzmann method given the medium properties $c(\mathbf{r})$ and the source function.

In the scattering theory, the forward problem is described differently. The scattering theory is a form of perturbation theory. That is, in the scattering theory, the actual medium is separated into two parts: One part is called the reference medium, and the other part is called the perturbation (the difference between the actual medium and the reference medium). In general, we can express the differential equations governing wave propagation in the actual medium and reference medium as

$$LG = -\delta(\mathbf{r} - \mathbf{r}_s) \tag{A-2}$$

and

$$L_0 G_0 = -\delta(\mathbf{r} - \mathbf{r}_s), \tag{A-3}$$

respectively. The terms L and L_0 are the general differential operators in the actual and reference medium, and G and G_0 are the actual and reference wavefields, respectively. The symbol δ is the Dirac delta source function, and $\mathbf{r}$ and $\mathbf{r}_s$ are the field and source locations, respectively. The perturbation differential operator is defined as $V \equiv L - L_0$. The differential operators L and L_0 contain the properties in the actual and the reference media that govern wave propagation in these media. Different earth model types are described by different forms of operators L and L_0. These operators contain the (spatially variant) parameters of the specific earth model type (e.g., acoustic, elastic, anisotropic, and anelastic). For example, for an acoustic, variable-velocity constant-density model type, $L = \nabla^2 + k^2$, where $k = \omega/c(\mathbf{r})$ as illustrated in equation A-1. The term $L_0 = \nabla^2 + k^2$, where $k_0 = \omega/c_0(\mathbf{r})$ as in $[\nabla^2 + k_0^2]G_0(\mathbf{r}, \mathbf{r}_s, \omega) = -\delta(\mathbf{r} - \mathbf{r}_s)$.

We can express the actual medium differential operator L in terms of a reference medium differential operator L_0 and a perturbation operator V as $L = L_0 + V$. The perturbation operator is defined as $V = L - L_0$. Thus, equation A-2 can be written as

$$(L_0 + V)G = -\delta. \tag{A-4}$$

Rearrange the above expression as follows:

$$\begin{aligned} L_0 G &= -\delta - VG, \\ G &= -L_0^{-1}\delta - L_0^{-1}VG. \end{aligned} \tag{A-5}$$

Now, substituting $\delta = -L_0 G_0$ (equation A-3) and considering $L_0^{-1} = -G_0$, we have

$$\begin{aligned} G &= L_0^{-1} L_0 G_0 - L_0^{-1} VG, \\ G &= G_0 + G_0 VG.. \end{aligned} \tag{A-6}$$

The above equation A-6 is called the Lippmann-Schwinger equation (e.g., Taylor, 1972). The Lippmann-Schwinger equation is an operator relationship among G (the wavefield in the actual medium), G_0 (the wavefield in the reference medium), and V (the perturbation). The symbol G appears on both sides of equation A-6. To solve equation A-6 for G, we can treat $G = G_0$ (the first term on the right-hand side of equation A-6) as a first approximation for G. Then, substituting $G = G_0$ on the right side of equation A-6, we find an approximation for G as $G_0 + G_0 V G_0$, and then once again we substitute this next approximation for G on the right side of equation A-6; we find an updated approximation for G:

$$G_0 + G_0 V G_0 + G_0 V G_0 V G_0. \tag{A-7}$$

Then, continuing this successive substitution process for G on the right side of equation A-6, we find

$$G = G_0 + G_0 V G_0 + G_0 V G_0 V G_0 + G_0 V G_0 V G_0 V G_0 + \cdots . \tag{A-8}$$

The difference between actual wavefield G and reference wavefield G_0 is defined as scattered wavefield $\psi_s = G - G_0$.

The seismic *forward* problem is solved in the scattering theory by equation A-8; i.e., given the reference wavefield G_0 and perturbation V (the right side of equation A-8), equation A-8 can be used as a forward-modeling tool to obtain the actual wavefield G (the left side of equation A-8). The forward problem determines G from L. In scattering theory, L is given by L_0 and V; therefore, G_0 and V enter the forward or seismic modeling series (equation A-8). In common with all modeling methods, modeling (or the forward problem) within scattering theory depends on first specifying the earth model type and then all the precise earth properties within that model type. The recorded seismic data correspond to the wavefield (G or ψ_s) recorded on the measurement surface.

The seismic inverse problem

The seismic *inverse* problem is to solve for the medium properties L in terms of recorded values of the wavefield on the measurement surface outside V and the source.

The seismic inverse problem is solved in scattering theory by first solving for V. Then, V is added to the reference medium operator L_0 to obtain the actual medium operator L. To know L is to know all the physical properties that govern wave propagation in the actual medium. To derive the inverse scattering method to solve for V, let's first return to the forward series (equation A-8). We note that equation A-8 has the form of a generalized geometric series (Weglein, 2017)

$$G - G_0 = S = ar + ar^2 + ar^3 + \cdots = \frac{ar}{1 - r}, \tag{A-9}$$

for $|r| < 1$, where we have identified in our simple algebraic geometric series analog $a = G_0$ and $r = VG_0$. If we label the terms on the right side of equation A-9 as $S_1 = ar, S_2 = ar^2, \ldots$, where S_n is the part of S that is nth order in r; then, equation A-9 becomes

$$S = S_1 + S_2 + S_3 + \cdots = \frac{ar}{1 - r}. \tag{A-10}$$

Solving equation A-10 for r, in terms of S/a, produces an inverse geometric series

$$r = \frac{S/a}{1+S/a} = S/a - (S/a)^2 + (S/a)^3 + \cdots,$$
$$= r_1 + r_2 + r_3 + \cdots, \quad \text{(A-11)}$$

when $|S/a| < 1$, where r_n is the portion of r that is nth order in S/a.

For the seismic inverse problem, we evaluate equation A-8 for sources and receivers on the measurement surface and we associate S with the recorded values of the scattered wavefield $S = (\psi_s)_{ms} = (G - G_0)_{ms}$, and the forward series follow from treating the forward solution as S in terms of V, and the inverse series as V in terms of S. The inverse series is the analog of equation A-11, where $r_1, r_2, \ldots$ are replaced with $V_1, V_2, \ldots$:

$$V = V_1 + V_2 + V_3 + \cdots, \quad \text{(A-12)}$$

where V_n is the portion of V that is nth order in the data D. The data D are the recorded values of ψ_s, that is, $(\psi_s)_{MS}$. Substituting equation A-12 into equation A-8 and evaluating both sides of equation A-8 on the measurement surface, and setting terms of equal order in the data equal, produces the following set of equations (see, e.g., Weglein et al., 2003):

$$(\psi_s)_{ms} = (G_0 V_1 G_0)_{ms}, \quad \text{(A-13)}$$

$$0 = (G_0 V_2 G_0)_{ms} + (G_0 V_1 G_0 V_1 G_0)_{ms}, \quad \text{(A-14)}$$

$$0 = (G_0 V_3 G_0)_{ms} + (G_0 V_2 G_0 V_1 G_0)_{ms} + (G_0 V_1 G_0 V_2 G_0)_{ms}$$
$$+ (G_0 V_1 G_0 V_1 G_0 V_1 G_0)_{ms}, \quad \text{(A-15)}$$

$$0 = (G_0 V_n G_0)_{ms} + (G_0 V_1 G_0 V_{n-1} G_0)_{ms} + \cdots$$
$$+ (G_0 V_1 G_0 V_1 G_0 V_1 \cdots G_0 V_1 G_0)_{ms}. \quad \text{(A-16)}$$

The term V_1 can be solved in equation A-13 using the measured scattered wavefield $(\psi_s)_{ms}$ and the reference wavefield G_0. Then, substitute V_1 into equation A-14 and solve for V_2 as in equation A-13. In this manner, we can compute any V_n only using the measured scattered wavefield $(\psi_s)_{ms}$ and the reference wavefield G_0. Hence, $V = \sum_{n=1}^{\infty} V_n$ is an explicit direct inversion solution and it does not require any subsurface information. The inverse step in equations A-13–A-16 when solving for $V_1, V_2, V_3, \ldots$ involves inverting the same unchanged operator G_0, and when the reference medium is homogeneous, that inverse step is analytic (Weglein et al., 2003).

The ISS methods were first developed by Moses (1956), Prosser (1969), and Razavy (1975). Weglein et al. (1981) and Stolt and Jacobs (1980) apply the ISS methods to extract multidimensional earth information from seismic data. Carvalho (1992) performs empirical tests of the ISS method for a normal-incident plane wave on a 1D acoustic medium. The result indicated that the full series only converges when the difference between the actual earth's acoustic velocity and reference velocity (the water velocity) is less than 11%. In response, the idea of isolated task-specific subseries was developed as a way to extract useful information from the only direct inversion method for a multidimensional subsurface. The isolated task ISS subseries are (1) FSME, (2) internal multiple attenuation/elimination, (3) Q compensation without knowing or estimating Q, (4) depth imaging, and (5) inversion (parameter estimation). The identification of the terms in the ISS to be included in a given task-specific subseries used several different types of analysis with testing of new concepts to evaluate, refine, and develop embryonic thinking based on forward series processes and analogs and a large dose of physical intuition (Weglein et al., 2003). For example, for free-surface multiples, understanding how the forward scattering series produces or generates a free-surface multiple event provides a "hint" of where the inverse process that removes that event might be located. That hint, due to a symmetry between event creation and event removal, turns out to be useful. For internal multiples, the location of terms that perform attenuation and elimination is described in Weglein et al. (2003, pp. R55–R62). For the purpose of this paper, it is useful to review the thinking behind locating the ISS subseries for removing free-surface multiples.

In the absence of a free surface (and choosing an infinite whole space of water as the reference medium), a forward series equation A-8 describing the data is constructed from the direct propagating Green's function G_0^d and the perturbation operator V. The symbol V represents the difference between the actual material properties of the world and the reference medium. The symbol V has nonzero values starting at the water bottom. In the presence of a free surface, let G_0^{fs} corresponds to the extra part of the Green's function due to a Dirac delta point source in the water column that propagates up and reflects off the free surface and has a field point below the free surface.

With the free surface present, the forward series is constructed from $G_0 = G_0^d + G_0^{fs}$ and the same perturbation operator V. Hence, G_0 with or without G_0^{FS} is the only difference between the forward series with and without the free surface. Therefore, G_0^{fs} is responsible for generating those events in the forward or modeling series that owe their existence to the presence of the free surface, i.e., ghosts and free-surface multiples. In the inverse series, equations A-13–A-16, it is reasonable to infer that G_0^{fs} will be responsible for all the extra tasks that inversion needs to perform when starting with data containing ghosts and free-surface multiples rather than data without those events. Those extra inverse tasks include deghosting and the removal of free-surface multiples.

The inverse series expansions, equations A-13–A-16, consist of terms $(G_0 V_n G_0)_m$ with $G_0 = G_0^d + G_0^{fs}$. Source and receiver deghosting is realized by removing the two outside $G_0 = G_0^d + G_0^{fs}$ functions and replacing them with G_0^d.

Data are considered the measured values of the scattered wavefield, equation A-13. The source- and receiver-deghosted data (represented by $\tilde{D}$) are related to V_1 as $\tilde{D} = (G_0^d V_1 G_0^d)_m$. After the deghosting operation, the objective is to remove the free-surface multiples from the deghosted data $\tilde{D}$.

The terms in the inverse series expansions, equations A-13–A-16, replacing D with input $\tilde{D}$, contain G_0^d and G_0^{fs} between the operators V_i. The outer G_0^ds (rather than $G_0 = G_0^d + G_0^{fs}$) indicate that the data have been source and receiver deghosted. The inner G_0^d and G_0^{fs} are where the five inversion tasks (free-surface multiple removal, internal multiple removal, depth imaging, Q compensation without knowing or estimating Q, and inversion/parameter estimation) reside. If we consider ISS and $G_0 = G_0^d + G_0^{fs}$, and if we assume that the data have been source and receiver deghosted (i.e., G_0^d replaces $(G_0^{fs} + G_0^d)$ on the outside of all terms), then the terms in the series are of three types:

$$\text{Type 1}: (G_0^d V_i G_0^{fs} V_j G_0^{fs} V_k G_0^d)_{ms}, \tag{A-17}$$

$$\text{Type 2}: (G_0^d V_i G_0^{fs} V_j G_0^{d} V_k G_0^d)_{ms}, \tag{A-18}$$

$$\text{Type 3}: (G_0^d V_i G_0^{d} V_j G_0^{d} V_k G_0^d)_{ms}. \tag{A-19}$$

We interpret these types of terms from a task isolation point of view. Type 1 terms have only G_0^{fs} between two V_i, V_j contributions; these terms when added to $\tilde{D}$ remove free-surface multiples and perform no other task. Type 2 terms have G_0^d and G_0^{fs} between two V_i, V_j contributions; these terms perform free-surface multiple removal *plus* a task associated with G_0^d. (Tasks that G_0^d will achieve are the following: internal multiple removal, Q compensation, depth imaging, and nonlinear direct parameter estimation.) Type 3 terms have only G_0^d between two V_i, V_j contributions; these terms do not remove any free-surface multiples. Type 2 terms are coupled tasks with a free surface and G_0^d tasks. The idea behind the task-separated subseries is twofold: (1) isolate the terms in the overall series that perform a given task *as if no other tasks exist* (e.g., type 1 above) and after performing that task on the data and (2) not to return to the original inverse series with its coupled tasks involving G_0^{fs} and G_0^d; rather, restart the problem with an input data free of free-surface multiples D'.

With the idea of isolated task-separated subseries, the subseries for removing free-surface multiples reside in type 1 terms. Collecting all type 1 terms, we have

$$D_1' \equiv \tilde{D} = (G_0^d V_1 G_0^d)_{ms}, \tag{A-20}$$

$$D_2' = (G_0^d V_2 G_0^d)_m = -(G_0^d V_1 G_0^{fs} V_1 G_0^d)_{ms}, \tag{A-21}$$

$$\begin{aligned} D_3' = &-(G_0^d V_1 G_0^{fs} V_1 G_0^{fs} V_1 G_0^d)_{ms} - (G_0^d V_2 G_0^{fs} V_1 G_0^d)_{ms} \\ &- (G_0^d V_1 G_0^{fs} V_2 G_0^d)_{ms} \cdots, \end{aligned} \tag{A-22}$$

where $D_1' \equiv \tilde{D}$ is the first term; it is the seismic data after the removal of the reference wave $G_0 = G_0^d + G_0^{FS}$ and then source and receiver deghosting the scattered wavefield.

The term D_3' can be simplified as (see, e.g., Weglein et al., 2003)

$$D_3' = (D_0^d V_1 G_0^{fs} V_1 G_0^{fs} V_1 G_0^d)_{ms}. \tag{A-23}$$

Equation A-20 can be expressed as follows:

$$\begin{aligned} D_1'(x_g,z_g,x_s,z_s,\omega) = &\int dx_1 dz_1 dx_2 dz_2 G_0^d(x_g,z_g,x_1,z_1,\omega) \\ &\times V_1(x_1,z_1,x_2,z_2,\omega) G_0^d(x_2,z_2,x_s,z_s,\omega). \end{aligned} \tag{A-24}$$

Following the Fourier transform convention defined in, e.g., Clayton and Stolt (1981) and Weglein et al. (2003)

$$D(k_g,k_s,\omega) = \iiint D(x_g,x_s,t) e^{ik_s x_s - ik_g x_g + i\omega t} dt dx_g dx_s. \tag{A-25}$$

Fourier transforming over x_g, x_s on both sides of equation A-24

$$\begin{aligned} D_1'(k_g,z_g,k_s,z_s,\omega) = &\int dx_1 dz_1 dx_2 dz_2 G_0^d(k_g,z_g,x_1,z_1,\omega) \\ &\times V_1(x_1,z_1,x_2,z_2,\omega) G_0^d(x_2,z_2,k_s,z_s,\omega). \end{aligned} \tag{A-26}$$

The terms $G_0^d(k_g,z_g,x_1,z_1,\omega)$ and $G_0^d(x_2,z_2,k_s,z_s,\omega)$ are (see, e.g., Clayton and Stolt, 1981)

$$\begin{aligned} G_0^d(k_g,z_g,x_1,z_1,\omega) &= -\frac{e^{-i(k_g x_1 - q_g|z_1 - z_g|)}}{2iq_g} \\ &= -\frac{e^{-i(k_g x_1 - q_g(z_1 - z_g))}}{2iq_g} \end{aligned} \tag{A-27}$$

and

$$\begin{aligned} G_0^d(x_2,z_2,k_s,z_s,\omega) &= -\frac{e^{i(k_s x_2 + q_s|z_2 - z_s|)}}{2iq_s} \\ &= -\frac{e^{i(k_s x_2 + q_s(z_2 - z_s))}}{2iq_s}, \end{aligned} \tag{A-28}$$

respectively. In equations A-27 and A-28, we have assumed $z_1 > z_g$ and $z_2 > z_s$ to remove the absolute value ($|z_1 - z_g| \to (z_1 - z_g)$, $|z_2 - z_s| \to (z_2 - z_s)$) in the Green's functions. This assumption corresponds to the assumption that the perturbation $V_1(x_1,z_1,x_2,z_2)$ is *below* (and larger than) the source z_s and receiver depth z_g (i.e., the measurement surface). The positive direction for z is pointing downward; hence, the perturbation being nonzero below the measurement surface means $z_1 > z_g$ and $z_2 > z_s$ for a nonzero V_1 contribution.

Substituting equations A-27 and A-28 into equation A-26, we have

$$\begin{aligned} D_1'(k_g,z_g,k_s,z_s,\omega) &= \int dx_1 dz_1 dx_2 dz_2 \frac{e^{-i(k_g x_1 - q_g(z_1 - z_g))}}{2iq_g} \\ &\quad \times V_1(x_1,z_1,x_2,z_2,\omega) \frac{e^{i(k_s x_2 + q_s(z_2 - z_s))}}{2iq_s} \\ &= \frac{e^{-iq_g z_g} e^{-iq_s z_s}}{2iq_g 2iq_s} V_1(k_g,q_q,k_s,q_s,\omega), \end{aligned} \tag{A-29}$$

where we recognize the integrals over x_1, z_1, x_2, z_2 as Fourier transforms.

Similarly, in equation A-21,

$$\begin{aligned} D_2'(x_g,z_g,x_s,z_s,\omega) = &(G_0^d(x_g,z_g,x_1,z_1) V_2(x_1,z_1,x_2,z_2,\omega) \\ &\times G_0^d(x_2,z_2,x_s,z_s,\omega))_{ms} \end{aligned} \tag{A-30}$$

can be expressed as

$$D_2'(k_g, z_g, k_s, z_s, \omega) = \frac{e^{-iq_g z_g} e^{-iq_s z_s}}{2iq_g 2iq_s} V_2(k_g, q_q, k_s, q_s \omega). \tag{A-31}$$

And for

$$\begin{aligned}&(G_0^d(x_g,z_g,x_1,z_1,\omega)V_2(x_1,z_1,x_2,z_2,\omega)G_0^d(x_2,z_2,x_s,z_s,\omega))_{ms} = \\ &-(G_0^d(x_g,z_g,x_1,z_1,\omega)V_1(x_1,z_1,x_2,z_2,\omega)G_0^{fs}(x_2,z_2,x_3,z_3,\omega) \\ &\times V_1(x_3,z_3,x_4,z_4,\omega)\times G_0^d(x_4,z_4,x_s,z_s,\omega))_{ms},\end{aligned} \tag{A-32}$$

the left side can be expressed as

$$\text{LHS} = \frac{e^{-iq_g z_g} e^{-iq_s z_s}}{2iq_g 2iq_s} V_2(k_g, q_q, k_s, q_s, \omega). \tag{A-33}$$

To solve for the right side of equation A-32, we have $G_0^d(k_g, z_g, x_1, z_1, \omega)$ and $G_0^d(x_2, z_2, k_s, z_s, \omega)$ expressed in equations A-27 and A-28, respectively. The term $G_0^{fs}(x_2, z_2, x_3, z_3, \omega)$ can be expressed as follows (see Figure A-1):

$$G_0^{fs}(x_2, z_2, x_3, z_3, \omega) = \frac{1}{2\pi} \int dk \frac{e^{ik(x_2-x_3)} e^{iq(z_2+z_3)}}{2iq}. \tag{A-34}$$

It should be noted that we have assumed that the free surface is at depth $z = 0$ in this expression. The right side now can be expressed as follows:

$$\begin{aligned}\text{RHS} &= -G_0^d V_1 G_0^{fs} V_1 G_0^d = -\int dx_1 dz_1 dx_2 dz_2 dx_3 dz_3 dx_4 dz_4 \\ &\times \frac{e^{-i(k_g x_1 - q_g(z_1 - z_g))}}{2iq_g} V_1(x_1, z_1, x_2, z_2, \omega) \frac{1}{2\pi} \\ &\times \int dk \frac{e^{ik(x_2-x_3)} e^{iq(z_2+z_3)}}{2iq} V_1(x_3, z_3, x_4, z_4, \omega) \\ &\times \frac{e^{i(k_s x_4 + q_s(z_4 - z_s))}}{2iq_s} = -\frac{e^{-iq_g z_g} e^{-iq_s z_s}}{2iq_g 2iq_s} \frac{1}{2\pi} \\ &\times \int dk V_1(k_g, q_q, k, q, \omega) \frac{1}{2iq} V_1(k, q, k_s, q_s, \omega).\end{aligned} \tag{A-35}$$

Canceling common factors on both sides (equations A-33 and A-35), we have

$$V_2(k_g, k_s, \omega) = -\frac{1}{2\pi} \int dk V_1(k_g, k, \omega) \frac{1}{2iq} V_1(k, k_s, \omega). \tag{A-36}$$

Substituting V_1 with D_1' using equation A-29 and V_2 with D_2' using equation A-31, we obtain the second term D_2' as follows:

$$D_2'(k_g, k_s, \omega) = -\frac{1}{2\pi} \int dk D_1(k_g, k, \omega)(2iq) e^{iq(z_g+z_s)} \times D_1(k, k_s, \omega). \tag{A-37}$$

In practice, equation A-37 is the free-surface elimination algorithm that directly inputs D_1 and outputs D_2'. Next, we show one example from Zhang (2007) to demonstrate that the ISS free-surface multiple-prediction algorithm predicts free-surface multiples with accurate time and amplitude.

Figure A-2 shows the model used to generate input data. The calculations are in the data domain: $V_1, V_2, \ldots$ are never solved for in ISS data-driven algorithms. The data contain the reference waves (yellow line), source and receiver ghosts (dashed blue line), free-surface multiples (black line), and primaries (red line). These data are first preprocessed by distinct Green's theorem methods to remove the reference waves and source and receiver ghosts. Then, the preprocessed data (consisting of primaries and free-surface multiples [for this example], see the solid line in Figure A-3) enter the ISS FSME algorithm. The result after ISS FSME is shown in Figure A-3 using a dashed line. The result after ISS FSME is obtained by $D_2' + D_1'$. When D_2' is added to D_1', two things happen: First-order free-surface multiples are eliminated, and all higher

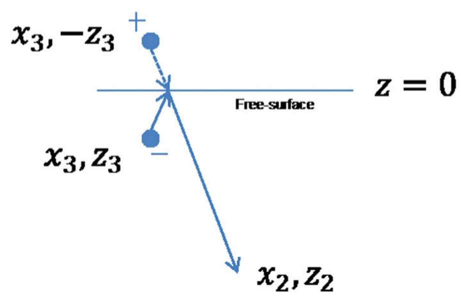

$$G_0^{fs}(x_2, z_2, x_3, z_3, \omega) = \frac{1}{2\pi} \int dk \frac{e^{ik(x_2-x_3)} e^{iq|z_2-(-z_3)|}}{2iq} = \frac{1}{2\pi} \int dk \frac{e^{ik(x_2-x_3)} e^{iq(z_2+z_3)}}{2iq}$$

Figure A-1. The Green's function G_0^{fs} travels up from the source to the free surface and then down to the receiver.

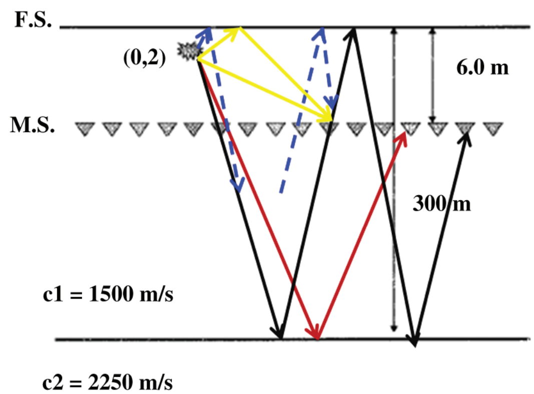

Figure A-2. The model used to generate data from Zhang (2007) to test the ISS FSME.

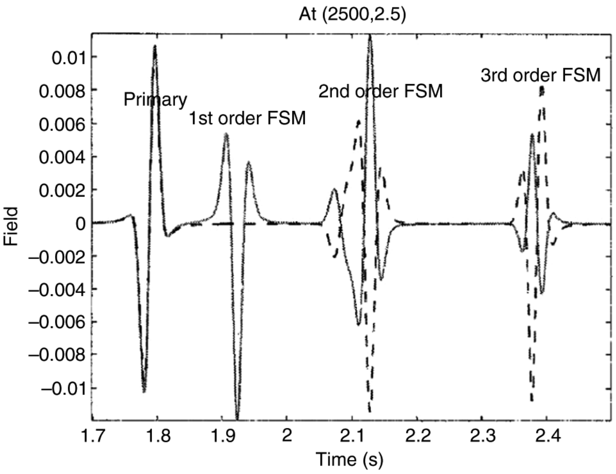

Figure A-3. A trace comparison between the input data D_1' (solid line) to the ISS FSME and output data $D_1' + D_2'$ after ISS FSME. When D_2' is added to D_1', two things happen: The first-order free-surface multiple is eliminated, and all higher order free-surface multiples are altered and are prepared for their removal by D_3', D_4', etc.

order free-surface multiples are altered and prepared for their removal by higher order terms in the ISS FSME subseries, D_3', D_4', etc.

APPENDIX B

COMPARING THE ISS FSME WITH SRME

In Appendix A, we have provided a brief derivation of the ISS FSME algorithm. The ISS FSME inputs seismic data that are generated by monopole sources (or source arrays) and that have the reference waves and source ghosts, receiver ghosts, and source-and-receiver ghosts all removed.

This algorithm predicts the exact time and exact amplitude of all free-surface multiples at all offsets. This provides a good starting point and opportunity to understand under what set of approximations we can derive the SRME prediction with its approximate prediction of the amplitude and phase of the free-surface multiples. This then locates and identifies the origin of the missing physics in the SRME prediction. It turns out that the SRME prediction corresponds to data with the reference waves removed and with source- and receiver-deghosted data, but where the source consists of a vertically separated dipole source in the water column. The vertically separated dipole source is defined as the limit of two vertically separately (of opposite sign) Dirac delta sources as the distance between them approaches zero and the source amplitude goes to infinity, in such a way that the product of the source amplitude and the distance between them remains constant. Because the data due to a vertically separated dipole source are not realizable in practice, the idea within SRME is to seek to approximate what a dipole source would produce by keeping the source-side ghost (see Figure B-1). That approximation and substitution are the origin of the missing or erroneous physics and result in an approximate prediction of the amplitude and phase of the free-surface multiples. We examine the consequence of that approximation and substitution on the exact ISS FSME prediction in this Appendix B.

Below we follow the SRME prescription to input the data with only the reference wave and receiver-side ghosts removed (i.e., keeping the source-side ghost). Under that SRME assumption, equations A-20 and A-21 become

$$D_1'' = (G_0^d V_1 (G_0^d + G_0^{fs}))_{ms}, \tag{B-1}$$

$$\begin{aligned} D_2'' &= (G_0^d V_2 (G_0^d + G_0^{fs}))_{ms} \\ &= -(G_0^d V_1 G_0^{fs} V_1 (G_0^d + G_0^{fs}))_{ms}. \end{aligned} \tag{B-2}$$

With

$$G_0^{fs}(x_2, z_2, k_s, z_s, \omega) = \frac{e^{i(k_s x_2 + q_s(z_2 + z_s))}}{2iq_s}. \tag{B-3}$$

Equation B-1 now becomes

$$\begin{aligned} &D_1''(k_g, z_g, k_s, z_s, \omega) \\ &= \frac{e^{-iq_g z_g}(e^{-iq_s z_s} - e^{iq_s z_s})}{2iq_g 2iq_s} V_1(k_g, q_q, k_s, q_s, \omega). \end{aligned} \tag{B-4}$$

The left part of equation B-2 becomes

$$\begin{aligned} &D_2''(k_g, z_g, k_s, z_s, \omega) \\ &= \frac{e^{-iq_g z_g}(e^{-iq_s z_s} - e^{iq_s z_s})}{2iq_g 2iq_s} V_2(k_g, q_q, k_s, q_s, \omega). \end{aligned} \tag{B-5}$$

The right part of equation B-2 becomes

$$\begin{aligned} &-\frac{e^{-iq_g z_g}(e^{-iq_s z_s} - e^{iq_s z_s})}{2iq_g 2iq_s} \frac{1}{2\pi} \int dk V_1(k_g, q_q, k, q, \omega) \frac{1}{2iq} \\ &\times V_1(k, q, k_s, q_s, \omega). \end{aligned} \tag{B-6}$$

We have

$$V_2(k_g, k_s, \omega) = -\frac{1}{2\pi} \int dk V_1(k_g, k, \omega) \frac{1}{2iq} V_1(k, k_s, \omega). \tag{B-7}$$

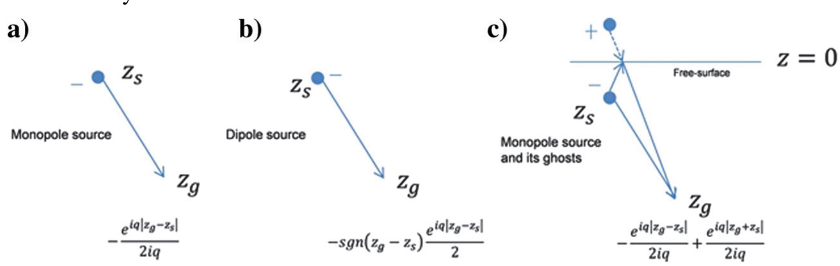

Figure B-1. (a) Monopole source and its 2D Green's function in the k_x, ω domain. (b) Dipole source and its 2D Green's function. (c) Monopole source and its source ghosts and their 2D Green's functions. The free surface is at a depth of $z = 0$. The term $q = \sqrt{(\omega^2/c_0) - k_x^2}$, where ω, k_x, and c_0 are the temporal frequency, horizontal wavenumber, and medium velocity, respectively.

Now, substituting V_1, V_2 with D_1'', D_2'' in equations B-4 and B-5, respectively, we have

$$D_2''(k_g, z_g, k_s, z_s, \omega) = \frac{1}{2\pi}\int dk D_1''(k_g, z_g, k, z_s, \omega) \frac{2iqe^{iqz_g}}{(e^{iqz_s} - e^{-iqz_s})} D_1''(k, z_g, k_s, z_s, \omega). \tag{B-8}$$

Let us take a look at the factor $(e^{iqz_s} - e^{-iqz_s})$ in the denominator. For a source that is close to the free surface (which means z_s is small because the free surface is assumed to be at a depth of $z = 0$ in this case), the factor $(e^{iqz_s} - e^{-iqz_s})$ can be approximated by

$$e^{iqz_s} - e^{-iqz_s} \approx iqe^{-iqz_s}2z_s. \tag{B-9}$$

Under this approximation, equation B-8 becomes

$$\begin{aligned} D_2''&(k_g, z_g, k_s, z_s, \omega) \\ &= \frac{1}{2\pi}\int dk D_1''(k_g, z_g, k, z_s, \omega)\frac{2iqe^{iqz_g}}{(e^{iqz_s} - e^{-iqz_s})} \\ &\times D_1''(k, z_g, k_s, z_s, \omega) \approx \frac{1}{2\pi}\int dk D_1''(k_g, z_g, k, z_s, \omega) \\ &\times (e^{iq(z_g+z_s)})D_1''(k, z_g, k_s, z_s, \omega)\frac{1}{z_s}. \end{aligned} \tag{B-10}$$

Now, if the receiver in the actual experiment is close to the free surface (z_g is small), then equation B-10 will be proportional to

$$\frac{1}{2\pi}\int dk D_1''(k_g, z_g, k, z_s, \omega) D_1''(k, z_g, k_s, z_s, \omega). \tag{B-11}$$

Applying the inverse Fourier transform on k_g and k_s, we have

$$\frac{1}{2\pi}\int dk D_1''(x_g, k, \omega) D_1''(k, x_s; \omega). \tag{B-12}$$

Expressing $D_1''(x_g, k, \omega)$ and $D_1''(k, x_s; \omega)$ using their Fourier transforms****

$$\frac{1}{2\pi}\int dk \underline{\int dx' D_1''(x_g, x'; \omega)e^{ikx'}}\, \underline{\int dx'' D_1''(x'', x_s; \omega)e^{-ikx''}}. \tag{B-13}$$

We rearrange the above equation

$$\frac{1}{2\pi}\int dx' \int dx'' D_1''(x_g, x'; \omega) D_1''(x'', x_s; \omega) \int dk e^{ik(x'-x'')}. \tag{B-14}$$

We have

$$\begin{aligned} &\frac{1}{2\pi}\int dx' \int dx'' D_1''(x_g, x'; \omega) D_1''(x'', x_s; \omega) \int dk e^{ik(x'-x'')} \\ &= \frac{1}{2\pi}\int dx' \int dx'' D_1''(x_g, x'; \omega) D_1''(x'', x_s; \omega)(2\pi\delta(x'-x'')) \\ &= \int dx D_1''(x_g, x; \omega) D_1''(x, x_s; \omega). \end{aligned} \tag{B-15}$$

We obtain the convolutional SRME free-surface-multiple prediction equation. Hence, the industry-standard free-surface algorithm, SRME, can be derived as an approximation to the ISS FSME algorithm. The ISS FSME predicts the exact time and amplitude of all free-surface multiples of different orders at all offsets. SRME predicts the approximate amplitude and phase of the free-surface multiples at all offsets.

REFERENCES

Amundsen, L., 1993, Wavenumber-based filtering of marine point-source data: Geophysics, **58**, 1335–1348, doi: 10.1190/1.1443516.

Berkhout, A. J., 1985, Seismic migration: Theoretical aspects: Elsevier Publishing Co.

Cagniard, L., 1939, Reflexion et refraction des ondes sismiques progressive: Gauthier-Villar.

Carvalho, P. M., 1992, Free-surface multiple reflection elimination method based on nonlinear inversion of seismic data: Ph.D. thesis, Universidade Federal da Bahia.

Carvalho, P. M., and A. B. Weglein, 1994, Wavelet estimation for surface multiple attenuation using a simulated annealing algorithm: 64th Annual International Meeting, SEG, Expanded Abstracts, 1481–1484, doi: 10.1190/1.1822816.

Carvalho, P. M., A. B. Weglein, and R. H. Stolt, 1991, Examples of a nonlinear inversion method based on the T-matrix of scattering theory: Application to multiple suppression: 61st Annual International Meeting, SEG, Expanded Abstracts, 1319–1322, doi: 10.1190/1.1889114.

Clayton, R. W., and R. H. Stolt, 1981, A Born-WKBJ inversion method for acoustic reflection data: Geophysics, **46**, 1559–1567, doi: 10.1190/1.1441162.

de Hoop, A. T., 1959, The surface line source problem: Applied Scientific Research B, **8**, 349–356.

Ferreira, A., 2011, Internal multiple removal in offshore Brazil seismic data using the inverse scattering series: Ph.D. thesis, University of Houston.

Kolsky, H., 1956, The propagation of stress waves in viscoelastic solids: Philosophical Magazine, **1**, 693–710, doi: 10.1080/14786435608238144.

Ma, C., and A. B. Weglein, 2016, Examining the interdependence and cooperation of the terms in the distinct inverse-scattering subseries for free-surface multiple and internal multiple removal: 86th Annual International Meeting, SEG, Expanded Abstracts, 4561–4565, doi: 10.1190/segam2016-13961170.1

Matson, K., D. Corrigan, A. B. Weglein, C. Y. Yong, and P. Carvalho, 1999, Inverse scattering internal multiple attenuation: Results from complex synthetic and field data examples: 69th Annual International Meeting, SEG, Expanded Abstracts, 1060–1063, doi: 10.1190/1.1820681.

Matson, K. H., 1997, An inverse-scattering series method for attenuating elastic multiples from multicomponent land and ocean bottom seismic data: Ph.D. thesis, University of British Columbia.

Mayhan, J. D., 2013, Wave-theoretic preprocessing to allow the inverse scattering series methods for multiple removal and depth imaging to realize their potential and impact: Methods, examples, and added value: Ph.D. thesis, University of Houston.

Mayhan, J. D., and A. B. Weglein, 2013, First application of Green's theorem-derived source and receiver deghosting on deep-water Gulf of Mexico synthetic (SEAM) and field data: Geophysics, **78**, no. 2, WA77–WA89, doi: 10.1190/geo2012-0295.1.

Moses, H. E., 1956, Calculation of the scattering potential from reflection coefficients: Physical Review, **102**, 559–567, doi: 10.1103/PhysRev.102.559.

Osen, A., B. G. Secrest, L. Amundsen, and A. Reitan, 1998, Wavelet estimation from marine pressure measurements: Geophysics, **63**, 2108–2119, doi: 10.1190/1.1444504.

Prosser, R. T., 1969, Formal solutions of inverse scattering problems: Journal of Mathematical Physics, **10**, 1819–1822, doi: 10.1063/1.1664766.

Razavy, M., 1975, Determination of the wave velocity in an inhomogeneous medium from the reflection coefficient: The Journal of the Acoustical Society of America, **58**, 956–963, doi: 10.1121/1.380756.
Shen, Y., 2017, Wave-theory-based seismic data preprocessing: An extension of the current deghosting method to allow for a variable measurement surface topography and its impact on the inverse scattering series multiple removal: Ph.D. thesis, University of Houston.
Stolt, R. H., and B. Jacobs, 1980, Inversion of seismic data in a laterally heterogeneous medium: Stanford Exploration Project 24, 135–152.
Stolt, R. H., and A. B. Weglein, 1985, Migration and inversion of seismic data: Geophysics, **50**, 2458–2472, doi: 10.1190/1.1441877.
Tan, T. H., 1999, Wavelet spectrum estimation: Geophysics, **64**, 1836–1846, doi: 10.1190/1.1444689.
Taylor, J. R., 1972, Scattering theory: The quantum theory of nonrelativistic collisions: John Wiley & Sons Inc.
Verschuur, D. J., 1991, Surface-related multiple elimination, an inversion approach: Ph.D. thesis, Delft University of Technology.
Verschuur, D. J., A. J. Berkhout, and C. P. A. Wapenaar, 1992, Adaptive surface-related multiple elimination: Geophysics, **57**, 1166–1177, doi: 10.1190/1.1443330.
Weglein, A. B., 2012, Short note: An alternative subtraction criteria (to energy minimization) for free-surface multiple removal: Mission-Oriented Seismic Research Program (M-OSRP) Annual Report.
Weglein, A. B., 2016, Multiples: Signal or noise?: Geophysics, **81**, no. 4, V283–V302, doi: 10.1190/geo2014-0486.1.
Weglein, A. B., 2017, A direct inverse method for subsurface properties: The conceptual and practical benefit and added value in comparison with all current indirect methods, for example, amplitude-variation-with-offset and full-waveform inversion: Interpretation, **5**, no. 3, SL89–SL107, doi: 10.1190/INT-2016-0198.1.
Weglein, A. B., 2018, University of Houston, http://www.mosrp.uh.edu/events/annual-meetings/meeting-18, accessed June 2018.
Weglein, A. B., 2018a, A new and comprehensive perspective on the role of primaries and multiples in seismic-data processing for structure determination and amplitude analysis: 88th Annual International Meeting, SEG, Expanded Abstracts, 4548–4552, doi: 10.1190/segam2018-2998334.1.
Weglein, A. B., 2018b, Direct and indirect inversion and a new and comprehensive perspective on the role of primaries and multiples in seismic data processing for structure determination and amplitude analysis: CT&F-Ciencia, Tecnologia y Futuro, **8**, no. 2, 5–21, doi: https://doi.org/10.29047/01225383.87.
Weglein, A. B., F. V. Araujo, P. M. Carvalho, R. H. Stolt, K. H. Matson, R. T. Coates, D. Corrigan, D. J. Foster, S. A. Shaw, and H. Zhang, 2003, Inverse scattering series and seismic exploration: Inverse Problems, **19**, R27–R83, doi: 10.1088/0266-5611/19/6/R01.
Weglein, A. B., W. E. Boyce, and J. E. Anderson, 1981, Obtaining three-dimensional velocity information directly from reflection seismic data: An inverse scattering formalism: Geophysics, **46**, 1116–1120, doi: 10.1190/1.1441252.
Weglein, A. B., and W. Dragoset, 2005, Multiple attenuation: SEG, Geophysics Reprint Series.
Weglein, A. B., F. A. Gasparotto, P. M. Carvalho, and R. H. Stolt, 1997, An inverse-scattering series method for attenuating multiples in seismic reflection data: Geophysics, **62**, 1975–1989, doi: 10.1190/1.1444298.
Weglein, A. B., K. H. Matson, and A. J. Berkhout, 2000, Wave theoretic approaches to multiple attenuation: Concepts, status, open issues, and plans — Part 2: Offshore Technology Conference, doi: https://doi.org/10.4043/12011-MS.
Weglein, A. B., and B. G. Secrest, 1990, Wavelet estimation for a multidimensional acoustic earth model: Geophysics, **55**, 902–913, doi: 10.1190/1.1442905.
Weglein, A. B., S. A. Shaw, K. H. Matson, J. L. Sheiman, R. H. Stolt, T. H. Tan, A. Osen, G. P. Correa, K. A. Innanen, Z. Guo, and J. Zhang, 2002, New approaches to deghosting towed-streamer and ocean-bottom pressure measurements: 72nd Annual International Meeting, SEG, Expanded Abstracts, 2114–2117, doi: 10.1190/1.1817121.
Wu, J., and A. B. Weglein, 2014, Elastic Green's theorem preprocessing for on-shore internal multiple attenuation: Theory and initial synthetic data tests: 84th Annual International Meeting, SEG, Expanded Abstracts, 4299–4304, doi: 10.1190/segam2014-1513.1.
Wu, J., and A. B. Weglein, 2015, Preprocessing in displacement space for on-shore seismic processing: Removing ground roll and ghosts without damaging the reflection data: 85th Annual International Meeting, SEG, Expanded Abstracts, 4626–4630.
Wu, J., and A. B. Weglein, 2016a, Green's theorem-based onshore preprocessing: A reduced data requirement assuming a vacuum/earth model for the air/earth interface and the evaluation of the usefulness of that assumption: 86th Annual International Meeting, SEG, Expanded Abstracts, 4685–4689, doi: 10.1190/segam2016-13956378.1.
Wu, J., and A. B. Weglein, 2016b, Predicting deghosted reflection data for both pressure and multicomponent displacements at the ocean bottom: 86th Annual International Meeting, SEG, Expanded Abstracts, 4751–4755, doi: 10.1190/segam2016-13868798.1.
Wu, J., and A. B. Weglein, 2017, A new method for deghosting data collected on a depth-variable acquisition surface by combining Green's theorem wave separation followed by a Stolt extended Claerbout III wave prediction for one-way propagating waves: 87th Annual International Meeting, SEG, Expanded Abstracts, 4859–4864, doi: 10.1190/segam2017-17748868.1.
Zhang, H., and S. Shaw, 2010, 1-D analytical analysis of higher order internal multiples predicted via the inverse scattering series based algorithm: 80th Annual International Meeting, SEG, Expanded Abstracts, 3493–3498, doi: 10.1190/1.3513575.
Zhang, J., 2007, Wave theory based data preparation for inverse scattering multiple removal, depth imaging and parameter estimation: Analysis and numerical tests of Green's theorem deghosting theory: Ph.D. thesis, University of Houston.
Zhang, Z., 2017, Impact of the topography of the acquisition surface on preprocessing and subsequent free surface multiple elimination and depth migration: Examining the issue and providing a preprocessing response that accommodates a variable topography — Thereby allowing subsequent multiple removal and imaging methods to deliver their promise and potential: Ph.D. thesis, University of Houston.